

Scalar versus fermionic top partner interpretations of $t\bar{t} + E_T^{\text{miss}}$ searches at the LHC

Sabine Kraml,^a Ursula Laa,^{a,b} Luca Panizzi,^{c,d} Hugo Prager^{c,d}

^a*Laboratoire de Physique Subatomique et de Cosmologie, Université Grenoble-Alpes, CNRS/IN2P3, 53 Avenue des Martyrs, F-38026 Grenoble, France*

^b*LAPTH, Université Savoie Mont Blanc, CNRS, B.P. 110, F-74941 Annecy-le-Vieux, France*

^c*School of Physics and Astronomy, University of Southampton, Highfield, Southampton SO17 1BJ, UK*

^d*Particle Physics Department, Rutherford Appleton Laboratory, Chilton, Didcot, Oxon OX11 0QX, UK*

E-mail: sabine.kraml@lpsc.in2p3.fr, ursula.laa@lpsc.in2p3.fr,
l.panizzi@soton.ac.uk, hugo.prager@soton.ac.uk

ABSTRACT: We assess how different ATLAS and CMS searches for supersymmetry in the $t\bar{t} + E_T^{\text{miss}}$ final state at Run 1 of the LHC constrain scenarios with a fermionic top partner and a dark matter candidate. We find that the efficiencies of these searches in all-hadronic, 1-lepton and 2-lepton channels are quite similar for scalar and fermionic top partners. Therefore, in general, efficiency maps for stop–neutralino simplified models can also be applied to fermionic top-partner models, provided the narrow width approximation holds in the latter. Owing to the much higher production cross-sections of heavy top quarks as compared to stops, masses up to $m_T \approx 850$ GeV can be excluded from the Run 1 stop searches. Since the simplified-model results published by ATLAS and CMS do not extend to such high masses, we provide our own efficiency maps obtained with CHECKMATE and MADANALYSIS 5 for these searches. Finally, we also discuss how generic gluino/squark searches in multi-jet final states constrain heavy top partner production.

Contents

1	Introduction	2
2	Benchmark scenarios	4
2.1	The SUSY case: stop–neutralino simplified model	4
2.2	The extra quark scenario: conventions and Lagrangian terms	5
2.3	Benchmark points	7
3	Monte Carlo event generation	8
3.1	Setup and tools	8
3.2	Generator-level distributions	10
4	Effects in existing 8 TeV analyses	12
4.1	Fully hadronic stop search	12
4.2	Stop search in the single lepton final state	14
4.3	Stop search in the 2-leptons final state	18
4.4	Gluino/squark search in the 2–6 jets final state	20
5	Results in the top-partner versus DM mass plane	22
6	Conclusions	26
A	Additional CheckMATE results	28
B	Experimental data	30

1 Introduction

After the discovery of the Higgs boson [1, 2], the quest for new physics beyond the Standard Model (SM) is arguably the most pressing open issue in particle physics. If this new physics is responsible for the dark matter (DM) of the universe in the form of weakly interacting massive particles, its signatures at the LHC and other future colliders are expected to be characterized by events with an excess of missing transverse energy, E_T^{miss} . An intense experimental effort is thus being made at the LHC to isolate such signatures, though no signal has been observed so far.¹

The prototype for a new physics model leading to E_T^{miss} signatures is R-parity conserving supersymmetry (SUSY), in particular the minimal supersymmetric standard model (MSSM) with a neutralino as the lightest supersymmetric particle (LSP) [3–5]. Indeed, a large number of searches for final states containing jets and/or leptons plus E_T^{miss} have been designed by the ATLAS and CMS SUSY groups [6, 7], and the interpretations of the results are typically limits in some SUSY simplified model. Examples are multi-jet + E_T^{miss} searches being interpreted as limits in the the gluino–neutralino mass plane, or searches for the $t\bar{t} + E_T^{\text{miss}}$ final state being interpreted in terms of stops decaying to top+neutralino.

The same searches can be used to put constraints on scenarios leading to final states with E_T^{miss} generated by the production of extra quarks (XQs) decaying to a bosonic DM candidate. This occurs for instance in Universal Extra Dimensions (UED) [8–12], Little Higgs models with T-parity [13–18], or generically any model with extra matter and a \mathbb{Z}_2 parity under which the SM particles are even and (part of) the new states are odd. A common feature of these models is that the new states have the same spin as their SM partners, while in SUSY the spins differ by half a unit.

In all these models, the lightest odd particle is a DM candidate which interacts with the SM states through new mediator particles. A crucial property of scenarios where the mediators are odd is that they can only be produced in pairs or in association with other odd particles. This is then followed by (cascade) decays into SM particles and the DM candidate. Since the spins in the decays are all correlated, if it was possible to identify the spin of the mediator, this would give information on the bosonic/fermionic nature of the DM candidate as well.

It is therefore interesting to ask how the current results from SUSY searches constrain other models of new physics that would lead to the same signatures, and how same-spin and different-spin scenarios could be distinguished should a signal

¹Of course, E_T^{miss} signatures cannot be univocally associated with the production of DM. Neutral long-lived particles which decay outside the detector would produce the very same signatures without being DM. However, the observation of a signature compatible with DM at the LHC would allow to focus on specific regions of the parameter space to be corroborated by other observations, like DM direct and/or indirect detection.

be observed. In this paper, we concentrate on the first of these questions, comparing the cases of pair production of scalar (SUSY) and fermionic (XQ) top partners with charge $2/3$, which decay into $t + \text{DM}$,² thus leading to a $t\bar{t} + E_T^{\text{miss}}$ final state. Concretely, we consider the processes

$$\begin{aligned} \text{Top partner with spin 0:} \quad & pp \rightarrow \tilde{t} \tilde{t}^* \rightarrow t\bar{t} + \tilde{\chi}^0 \tilde{\chi}^0 \\ \text{Top partner with spin 1/2:} \quad & pp \rightarrow T \bar{T} \rightarrow t\bar{t} + \{S^0 S^0 \text{ or } V^0 V^0\} \end{aligned}$$

where $\tilde{\chi}^0$, S^0 and V^0 represent fermionic, scalar, and vectorial DM candidates respectively. Recasting a number of ATLAS and CMS searches for stops [19–22] from Run 1 of the LHC, as well as a generic search for gluinos and squarks [23] by means of CHECKMATE [24] and MADANALYSIS 5 [25, 26], we compare the efficiencies of these searches for the processes above. This allows us to determine whether cross-section upper limit maps or efficiency maps derived in the context of stop–neutralino simplified models can safely be applied to XQ scenarios where the $t\bar{t} + E_T^{\text{miss}}$ final state arises from the production of heavy T quarks. Such maps are used in public tools like SModelS [27, 28] and XQCAT [29, 30], and it is relevant to know how generically they can be applied. Moreover, we determine up-to-date bounds in the parameter space of the XQ and DM masses – such bounds were posed by a few early searches at the Tevatron [31, 32] and the LHC at 7 TeV [33, 34], but can be improved by a reinterpretation of the 8 TeV LHC results as we do in this paper.

Related studies exist in the literature. In particular, a re-interpretation of a few ATLAS and CMS SUSY searches at 7 TeV in terms of UED signatures was done in [35], using among others a simplified scenario with top-partners decaying to DM and light quarks. The applicability of SUSY simplified model results to new physics scenarios with same-spin SM partners was analysed in [36] also in the context of UED, focussing on the so-called T2 topology which corresponds to squark-antisquark production in the limit of a heavy gluino. The effect of a different spin structure for the $l^+ l^- + E_T^{\text{miss}}$ final state was studied in [37]. Recently, a study of constraints and LHC signatures of a scenario with a vector-like top partner decaying to a top quark and scalar DM has been performed in [38]. Here, we extend these works by considering specifically top partners and by applying up-to-date recasting tools.

The structure of the paper is the following. In Section 2, we describe the simplified models we use for the SUSY and XQ scenarios and define the benchmark points we consider for our analysis. The tools we use and the processes we consider are described in Section 3, together with selected kinematical distributions at generator level which are useful for a better understanding of our results. Section 4 provides detailed descriptions of the experimental analyses and the effects found for our benchmark points. The results are then summarized in the top-partner versus DM mass

²Here and in the following, we understand “DM” as the dark matter *candidate*, i.e. a neutral massive particle that escapes detection as E_T^{miss} but whose astrophysical properties remain open.

plane in Section 5. Section 6 contains our conclusions. A few additional results and comparisons which may be interesting to the reader are presented in Appendix A. The event numbers from the experimental analyses are listed in Appendix B.

2 Benchmark scenarios

2.1 The SUSY case: stop–neutralino simplified model

The prototype for the $t\bar{t} + E_T^{\text{miss}}$ signature in the SUSY context is a stop–neutralino simplified model. This assumes that the lighter stop, \tilde{t}_1 , and the lightest neutralino, $\tilde{\chi}_1^0$, taken to be the lightest SUSY particle and the DM candidate, are the only accessible sparticles — all other sparticles are assumed to be heavy. In this case, direct stop pair production is the only relevant SUSY production mechanism. Moreover, for large enough mass difference, the \tilde{t}_1 decays to 100% into $t + \tilde{\chi}_1^0$. The process we consider thus is

$$pp \rightarrow \tilde{t}_1 \tilde{t}_1^* \rightarrow t\bar{t} \tilde{\chi}_1^0 \tilde{\chi}_1^0. \quad (2.1)$$

Following the notation of [39], the top–stop–neutralino interaction is given by ($i = 1, 2$; $k = 1, \dots, 4$)

$$\begin{aligned} \mathcal{L}_{t\tilde{t}\tilde{\chi}^0} &= g \bar{t} (f_{Lk}^{\tilde{t}} P_R + h_{Lk}^{\tilde{t}} P_L) \tilde{\chi}_k^0 \tilde{t}_L + g \bar{t} (h_{Rk}^{\tilde{t}} P_R + f_{Rk}^{\tilde{t}} P_L) \tilde{\chi}_k^0 \tilde{t}_R + \text{h.c.} \\ &= g \bar{t} (a_{ik}^{\tilde{t}} P_R + b_{ik}^{\tilde{t}} P_L) \tilde{\chi}_k^0 \tilde{t}_i + \text{h.c.} \end{aligned} \quad (2.2)$$

where $P_{R,L} = \frac{1}{2}(1 \pm \gamma_5)$ are the right and left projection operators, and

$$\begin{aligned} a_{ik}^{\tilde{t}} &= f_{Lk}^{\tilde{t}} R_{i1}^{\tilde{t}} + h_{Rk}^{\tilde{t}} R_{i2}^{\tilde{t}}, \\ b_{ik}^{\tilde{t}} &= h_{Lk}^{\tilde{t}} R_{i1}^{\tilde{t}} + f_{Rk}^{\tilde{t}} R_{i2}^{\tilde{t}}. \end{aligned} \quad (2.3)$$

The $f_{L,R}^{\tilde{t}}$ and $h_{L,R}^{\tilde{t}}$ couplings are

$$\begin{aligned} f_{Lk}^{\tilde{t}} &= -\frac{1}{\sqrt{2}} (N_{k2} + \frac{1}{3} \tan \theta_W N_{k1}), \\ f_{Rk}^{\tilde{t}} &= \frac{2\sqrt{2}}{3} \tan \theta_W N_{k1}, \quad h_{Rk}^{\tilde{t}} = -y_t N_{k4} = h_{Lk}^{\tilde{t}*}, \end{aligned} \quad (2.4)$$

with N the neutralino mixing matrix and $y_t = m_t/(\sqrt{2}m_W \sin \beta)$ the top Yukawa coupling in the MSSM. Finally, R is the stop mixing matrix,

$$\begin{pmatrix} \tilde{t}_1 \\ \tilde{t}_2 \end{pmatrix} = R \begin{pmatrix} \tilde{t}_L \\ \tilde{t}_R \end{pmatrix}, \quad R = \begin{pmatrix} \cos \theta_{\tilde{t}} & \sin \theta_{\tilde{t}} \\ -\sin \theta_{\tilde{t}} & \cos \theta_{\tilde{t}} \end{pmatrix}. \quad (2.5)$$

All this follows SLHA [40] conventions.

Under the above assumption that all other neutralinos besides the $\tilde{\chi}_1^0$ and the charginos are heavy, the $\tilde{\chi}_1^0$ is dominantly a bino. Neglecting the wino and higgsino components N_{12} and N_{14} , the $t\bar{t}_1 \tilde{\chi}_1^0$ interaction from Eq. (2.2) simplifies to

$$\mathcal{L}_{t\bar{t}_1 \tilde{\chi}_1^0} \approx -\frac{g}{3\sqrt{2}} \tan \theta_W N_{11} \bar{t} (\cos \theta_{\tilde{t}} P_R - 4 \sin \theta_{\tilde{t}} P_L) \tilde{\chi}_1^0 \tilde{t}_1 + \text{h.c.} \quad (2.6)$$

While in practice one never has a *pure* bino, this approximation shows that the polarisation of the tops originating from the $\tilde{t}_1 \rightarrow t\tilde{\chi}_1^0$ decays will reflect the chirality of the \tilde{t}_1 . (The wino interaction also preserves the chirality, while the higgsino one flips it.) This will be relevant for defining XQ benchmark scenarios analogous to SUSY ones, since the p_T and angular distributions of the top decay products somewhat depend on the top polarisation [41–51].

2.2 The extra quark scenario: conventions and Lagrangian terms

As the XQ analogue of the SUSY case above, we consider a minimal extension of the SM with one extra quark state and one DM state, assuming that the XQ mediates the interaction between the DM and the SM quarks of the third generation. Interactions between the XQ, DM and lighter quarks are neglected. The most general Lagrangian terms depend on the representation of the DM and of the XQ. We label XQ singlet states as T (with charge $+2/3$) or B (with charge $-1/3$) and XQ doublet states as Ψ_Y , where Y corresponds to the weak hypercharge of the doublet in the convention $Q = T_3 + Y$, with Q the electric charge and T_3 the weak isospin. The doublets can then be $\Psi_{1/6} = \begin{pmatrix} T \\ B \end{pmatrix}$ or states which contain exotic components $\Psi_{7/6} = \begin{pmatrix} X_{5/3} \\ T \end{pmatrix}$ and $\Psi_{-5/6} = \begin{pmatrix} B \\ Y_{-4/3} \end{pmatrix}$. The DM states are labelled as S_{DM}^0 if scalar singlets or $V_{\text{DM}}^{0\mu}$ if vector singlets; if the DM belongs to a doublet representation, the multiplet is labelled as $\Sigma_{\text{DM}} = \begin{pmatrix} S_{\text{DM}}^+ \\ S_{\text{DM}}^0 \end{pmatrix}$ (with the charge conjugate $\Sigma_{\text{DM}}^c = \begin{pmatrix} S_{\text{DM}}^0 \\ -S_{\text{DM}}^- \end{pmatrix}$) if scalar or $\mathcal{V}_{\text{DM}} = \begin{pmatrix} V_{\text{DM}}^+ \\ V_{\text{DM}}^0 \end{pmatrix}$ (with the charge conjugate $\mathcal{V}_{\text{DM}}^c = \begin{pmatrix} V_{\text{DM}}^0 \\ V_{\text{DM}}^- \end{pmatrix}$) if vector. The couplings between the XQ, the DM and the SM quarks are denoted as λ_{ij}^q if the DM is scalar, or g_{ij}^q if the DM is vector: the labels $\{i, j\} = 1, 2$ indicate the representations of the XQ and DM respectively (1 for singlet, 2 for doublet), while $q = t, b$ identifies which SM quark the new states are coupled with, in case of ambiguity. We classify below the Lagrangian terms for the minimal SM extensions with one XQ and one DM representation (singlets and doublets) but we anticipate that in the following, for simplicity, we will only consider scenarios with a DM singlet.

- Lagrangian terms for a *DM singlet*. A DM singlet can couple either with a XQ singlet or with a XQ doublet $\Psi_{1/6} = \begin{pmatrix} T \\ B \end{pmatrix}$.

$$\mathcal{L}_1^S = \left[\lambda_{11}^t \bar{T} P_R t + \lambda_{11}^b \bar{B} P_R b + \lambda_{21} \bar{\Psi}_{1/6} P_L \begin{pmatrix} t \\ b \end{pmatrix} \right] S_{\text{DM}}^0 + \text{h.c.} \quad (2.7)$$

$$\mathcal{L}_1^V = \left[g_{11}^t \bar{T} \gamma_\mu P_R t + g_{11}^b \bar{B} \gamma_\mu P_R b + g_{21} \bar{\Psi}_{1/6} \gamma_\mu P_L \begin{pmatrix} t \\ b \end{pmatrix} \right] V_{\text{DM}}^{0\mu} + \text{h.c.} \quad (2.8)$$

- Lagrangian terms for a *DM doublet*. A DM doublet can couple with XQ singlets

or doublets with different hypercharges.

$$\begin{aligned}\mathcal{L}_2^S = & \left[\lambda_{12}^b \bar{B} P_L \begin{pmatrix} t \\ b \end{pmatrix} + \lambda_{22}^b \bar{\Psi}_{1/6} P_R b + (\lambda_{22}^t)' \bar{\Psi}_{5/6} P_R t \right] \Sigma_{\text{DM}} \\ & + \left[\lambda_{12}^t \bar{T} P_L \begin{pmatrix} t \\ b \end{pmatrix} + \lambda_{22}^t \bar{\Psi}_{1/6} P_R t + (\lambda_{22}^b)' \bar{\Psi}_{-1/6} P_R b \right] \Sigma_{\text{DM}}^c\end{aligned}\quad (2.9)$$

$$\begin{aligned}\mathcal{L}_2^V = & \left[g_{12}^b \bar{B} \gamma_\mu P_L \begin{pmatrix} t \\ b \end{pmatrix} + g_{22}^b \bar{\Psi}_{1/6} \gamma_\mu P_R b + (g_{22}^t)' \bar{\Psi}_{5/6} \gamma_\mu P_R t \right] \mathcal{V}_{\text{DM}}^\mu \\ & + \left[g_{12}^t \bar{T} \gamma_\mu P_L \begin{pmatrix} t \\ b \end{pmatrix} + g_{22}^t \bar{\Psi}_{1/6} \gamma_\mu P_R t + (g_{22}^b)' \bar{\Psi}_{-1/6} \gamma_\mu P_R b \right] \mathcal{V}_{\text{DM}}^{c,\mu}\end{aligned}\quad (2.10)$$

However, in scenarios with a DM doublet, there are always additional exotic states besides the XQ partners of the SM quarks and the DM state, namely charged scalars or vectors and quarks with charges 5/3 or 4/3. As mentioned above, in order to stick to a minimal extension of the SM containing a partner of the top quark and the DM candidate as the only new states, in the following we consider only the Lagrangian terms of Eqs. (2.7) or (2.8), depending on the spin of the DM. It is also worth noticing that in the considered scenarios the XQs do not mix with SM states because they have a different quantum number under the \mathcal{Z}_2 symmetry. Moreover, to focus only on top partners, we set $\lambda_{11}^b = g_{11}^b = 0$. Depending on the representation of the XQ, one can then identify some limiting cases:

- *Vector-like XQ (VLQ)*. If the XQ is vector-like, the left-handed and right-handed projections belong to the same $SU(2)$ representation. Therefore if the VLQ is a singlet, only couplings with SM singlets are allowed, and $\lambda_{21} = 0$ or $g_{21} = 0$. On the other hand, if the VLQ is a doublet, $\lambda_{11} = 0$ or $g_{11} = 0$. Unlike cases where VLQs mix with the SM quarks through Yukawa couplings via the Higgs boson, couplings for the opposite chiralities are not just suppressed, they are identically zero. The mass term for a VLQ can be written in a gauge-invariant way as:

$$\mathcal{L}_{\text{VLQ}} = -M_{T_{\text{VLQ}}} \bar{T} T \quad (2.11)$$

where $M_{T_{\text{VLQ}}}$ is a new physics mass scale not necessarily related to a Higgs-like mechanism for mass generation.

- *Chiral XQ (ChQ)*. If the XQ is chiral, all the couplings of Eqs. (2.7) or (2.8) can be allowed at the same time. ChQs can acquire mass in a gauge invariant way via the Higgs mechanism, analogously to SM quarks:

$$\begin{aligned}\mathcal{L}_{\text{ChQ}} = & -y_{\text{XQ}}^B \bar{\Psi}_{1/6} H B - y_{\text{XQ}}^T \bar{\Psi}_{1/6} H^c T + \text{h.c.} \\ \implies & -M_{T_{\text{ChQ}}} \bar{T} T - M_{B_{\text{ChQ}}} \bar{B} B\end{aligned}\quad (2.12)$$

where $M_{\{T,B\}_{\text{ChQ}}} = y_{\text{XQ}}^{\{T,B\}} v / \sqrt{2}$ and v is the Higgs VEV. At this point it has to be mentioned that the contribution of the new ChQ to Higgs production and

decay processes, even if different from scenarios where a 4th chiral generation mixes with the SM quarks, can be used to pose constraints on the coupling between the XQ and the Higgs boson, and as a consequence, on the maximum mass the ChQ can acquire through the Higgs mechanism. Of course, ChQs can still acquire mass by some different new physics mechanism (for example by interacting with a heavier scalar which develops a VEV). For this reason we can consider the ChQ mass as a free parameter in the following analysis.

2.3 Benchmark points

In order to compare the XQ and SUSY scenarios, it is useful to consider benchmark points with the same top-partner and DM masses as well as the same left and right couplings (leading to t_L or t_R in the final state) for the two models. To this end, we start from the stop-neutralino simplified model and choose two mass combinations: $(m_{\tilde{t}_1}, m_{\tilde{\chi}_1^0}) = (600, 10)$ GeV and $(m_{\tilde{t}_1}, m_{\tilde{\chi}_1^0}) = (600, 300)$ GeV. The first one is excluded by the 8 TeV searches, while the second one lies a bit outside the 8 TeV bounds [21, 52–55].³ Moreover, since the searches for $\tilde{t}_1 \rightarrow t\tilde{\chi}_1^0$ exhibit a small dependence on the top polarisation [20], we consider the two cases $\tilde{t}_1 \sim \tilde{t}_R$ and $\tilde{t}_1 \sim \tilde{t}_L$.⁴ The results for arbitrary stop mixing (or top polarisation) will then always lie between these two extreme cases. This leads to four benchmark scenarios, which we denote by

$$(600, 10)L; \quad (600, 10)R; \quad (600, 300)L; \quad (600, 300)R.$$

The strategy then is to use the same mass combinations (m_T, m_{DM}) and left/right couplings for the XQ case. For XQ+ S_{DM}^0 , we directly use $\lambda_{11}^t = b_{11}^t$ and $\lambda_{21}^t = a_{11}^t$. For XQ+ V_{DM}^0 , however, the width of the XQ would be too large if we were using the same parameters as in the SUSY or scalar DM case; to preserve the narrow width approximation, we therefore reduce the couplings by a factor 10, i.e. $g_{11}^t = b_{11}^t/10$ and $g_{21}^t = a_{11}^t/10$. The concrete values for the different benchmark scenarios are listed in Table 1.

The alert reader will notice that in Table 1, although there is a strong hierarchy between the left and right couplings, both of them are non-zero. Moreover, the couplings for the (600, 300)L case are not the same as for the (600, 10)L case; the same is true for (600, 300)R vs. (600, 10)R. The reason for this is as follows. The pure left or pure right case, $\tilde{t}_1 \equiv \tilde{t}_L$ or \tilde{t}_R , would require that the off-diagonal entry in the stop mixing matrix is exactly zero, that is $A_t \equiv \mu/\tan\beta$, where A_t is the trilinear stop-Higgs coupling, μ is the higgsino mass parameter and $\tan\beta = v_2/v_1$ is

³The $(m_{\tilde{t}_1}, m_{\tilde{\chi}_1^0}) = (600, 300)$ GeV mass combination actually lies just on the edge of the new 13 TeV bounds presented by CMS [56] at the Moriond 2016 conference.

⁴Strictly speaking, because of SU(2), a $\tilde{t}_1 \sim \tilde{t}_L$ should be accompanied by a \tilde{b}_L of similar mass; with no other 2-body decay being kinematically open, the sbottom would however decay to 100% into $b\tilde{\chi}_1^0$ and thus not contribute to the $t\bar{t} + E_T^{\text{miss}}$ signature.

	(600, 10)L		(600, 300)L	
$\tilde{t}_1 \sim \tilde{t}_L$	$a_{11}^{\tilde{t}} = -8.3649 \cdot 10^{-2}$	$b_{11}^{\tilde{t}} = 1.5406 \cdot 10^{-3}$	$a_{11}^{\tilde{t}} = -8.3638 \cdot 10^{-2}$	$b_{11}^{\tilde{t}} = 2.5811 \cdot 10^{-3}$
$XQ + S_{DM}^0$	$\lambda_{21}^{\tilde{t}} = -8.3649 \cdot 10^{-2}$	$\lambda_{11}^{\tilde{t}} = 1.5406 \cdot 10^{-3}$	$\lambda_{21}^{\tilde{t}} = -8.3638 \cdot 10^{-2}$	$\lambda_{11}^{\tilde{t}} = 2.5811 \cdot 10^{-3}$
$XQ + V_{DM}^0$	$g_{21}^{\tilde{t}} = -8.3649 \cdot 10^{-3}$	$g_{11}^{\tilde{t}} = 1.5406 \cdot 10^{-4}$	$g_{21}^{\tilde{t}} = -8.3638 \cdot 10^{-3}$	$g_{11}^{\tilde{t}} = 2.5811 \cdot 10^{-4}$
	(600, 10)R		(600, 300)R	
$\tilde{t}_1 \sim \tilde{t}_R$	$a_{11}^{\tilde{t}} = 1.1425 \cdot 10^{-3}$	$b_{11}^{\tilde{t}} = 3.3467 \cdot 10^{-1}$	$a_{11}^{\tilde{t}} = 2.1823 \cdot 10^{-3}$	$b_{11}^{\tilde{t}} = 3.3466 \cdot 10^{-1}$
$XQ + S_{DM}^0$	$\lambda_{21}^{\tilde{t}} = 1.1425 \cdot 10^{-3}$	$\lambda_{11}^{\tilde{t}} = 3.3467 \cdot 10^{-1}$	$\lambda_{21}^{\tilde{t}} = 2.1823 \cdot 10^{-3}$	$\lambda_{11}^{\tilde{t}} = 3.3466 \cdot 10^{-1}$
$XQ + V_{DM}^0$	$g_{21}^{\tilde{t}} = 1.1425 \cdot 10^{-4}$	$g_{11}^{\tilde{t}} = 3.3467 \cdot 10^{-2}$	$g_{21}^{\tilde{t}} = 2.1823 \cdot 10^{-4}$	$g_{11}^{\tilde{t}} = 3.3466 \cdot 10^{-2}$

Table 1. Benchmark points for the SUSY and XQ scenarios.

the ratio of the Higgs vacuum expectation values. To avoid such tuning, and also because the $\tilde{\chi}_1^0$ will never be a 100% pure bino even if the winos and higgsinos are very heavy, we refrain from using the approximation of Eq. (2.6) with $N_{11} = 1$ and $\cos \theta_{\tilde{t}} = 1$ or 0. Instead, we choose the masses of the benchmark points as desired by appropriately adjusting the relevant soft terms while setting all other soft masses to 3–5 TeV. From this we then compute the stop and neutralino mixing matrices and the full $\tilde{\chi}_1^0 \tilde{t}_1 t$ couplings $a_{11}^{\tilde{t}}$ and $b_{11}^{\tilde{t}}$ of Eq. (2.2), using SUSPECT v2.41 [57]. The resulting values are $N_{11} \simeq 1$, $\cos \theta_{\tilde{t}} \simeq 1$ (or $\sin \theta_{\tilde{t}} \simeq 1$) to sub-permil precision, but nonetheless this leads to a small non-zero value of the “other” sub-dominant coupling, and to a slight dependence on the $\tilde{\chi}_1^0$ mass. An interesting consequence is that our comparison between SUSY and XQ is effectively between SUSY and ChQ scenarios. A comparison between SUSY and VLQ scenarios would require $\tilde{t}_1 \equiv \tilde{t}_L$ or $\tilde{t}_1 \equiv \tilde{t}_R$. Our conclusions however do not depend on this.

3 Monte Carlo event generation

3.1 Setup and tools

For the Monte Carlo analysis, we simulate the $2 \rightarrow 6$ process

$$pp \rightarrow t \bar{t} \text{ DM DM} \rightarrow (W^+ b)(W^- \bar{b}) \text{ DM DM}$$

with MADGRAPH 5 [58, 59], where DM is the neutralino in the SUSY scenario or the scalar/vector boson in the XQ scenario. This preserves the spin correlations in the $t \rightarrow Wb$ decay. Events are then passed to PYTHIA 6 [60], which takes care of the decay $W \rightarrow 2f$ as well as hadronisation and parton showering.⁵

For the SUSY scenarios we make use of the MSSM model file in MADGRAPH, while for the XQ simulation we implemented the model in FEYNRULES [62] to obtain the UFO model format to be used inside MADGRAPH. For the PDFs we employ the

⁵In [61] it was argued that certain kinematic distributions show sizeable differences between LO and NLO, which can be ameliorated by including initial state radiation of extra jets. We tested this but did not find any relevant differences with and without simulating extra jets for the analyses we consider in this paper. We therefore conclude that LO matrix element plus parton showering is sufficient for the scope of this study, in particular as it saves a lot of CPU time.

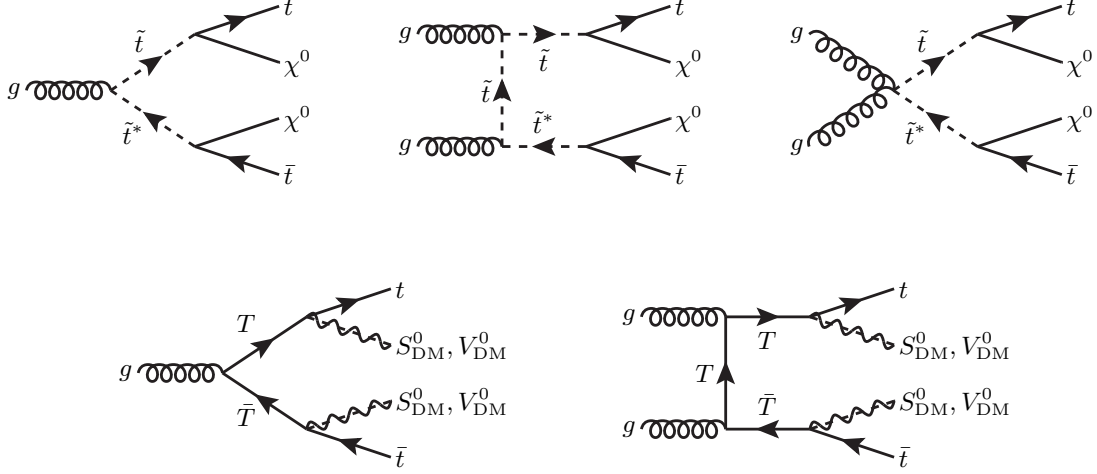


Figure 1. Feynman diagrams for the production of $t\bar{t} + E_T^{\text{miss}}$ in the SUSY and XQ scenarios. We have omitted for simplicity the $g\bar{g}$ and $q\bar{q}$ initial states which are common for the s-channel gluon topologies.

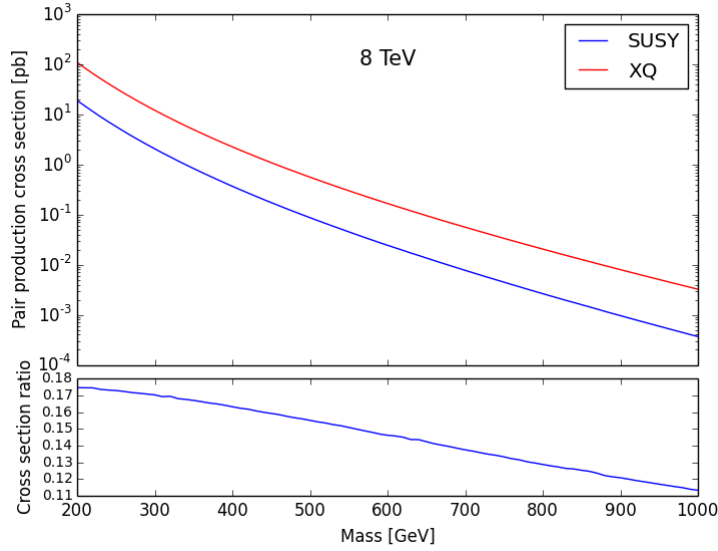


Figure 2. Production cross-sections for SUSY and XQ top partners at $\sqrt{s} = 8$ TeV.

cteq6l1 set [63]. To analyse and compare the effects of various ATLAS and CMS 8 TeV analyses, we employ CHECKMATE [24] as well as MADANALYSIS 5 [25]. Both frameworks use DELPHES 3 [64] for the emulation of detector effects.

The Feynman diagrams relevant for the SUSY and XQ processes are shown in Fig. 1. We observe that besides the difference in the spin of the mediator and DM, in the SUSY case there is a topology which is not present in the XQ case, namely the 4-leg diagram initiated by two gluons. The $pp \rightarrow \tilde{t}_1 \tilde{t}_1^*$ and $pp \rightarrow T\bar{T}$ production cross-sections at $\sqrt{s} = 8$ TeV are compared in Fig. 2. The comparison is done

at the highest available order for each scenario, i.e. at NLO+NLL for SUSY [65–72] and at NLO+NNLL for XQ [73]. We see that, for the same mass, the XQ cross-section is about a factor 5–10 larger than the SUSY cross-section. The same experimental analysis targeting $t\bar{t} + E_T^{\text{miss}}$ will therefore have a significantly higher reach in fermionic (XQ) than in scalar (SUSY) top partner masses. For instance, an excluded cross-section of 20 fb corresponds to $m_{\tilde{t}_1} \gtrsim 620$ GeV in the SUSY case but $m_T \gtrsim 800$ GeV in the XQ case. The precise reach will, of course, depend on the specific cut acceptances in the different models.

3.2 Generator-level distributions

As a first check whether we can expect specific differences in the cut efficiencies between the SUSY and XQ models, it is instructive to consider some basic parton-level distributions, as shown in Fig. 3 for the (600, 10) mass combination. These distributions have been obtained using MADANALYSIS 5 and considering the showered and hadronised event files from PYTHIA; jets have been processed through FASTJET [74, 75] using the anti-kt algorithm with minimum $p_T = 5$ GeV and cone radius $R = 0.5$. We see that the SUSY events tend to have more jets and a slightly harder E_T^{miss} spectrum. Moreover, the leading and sub-leading jets tend to be somewhat harder in the SUSY than in the XQ cases. Overall, these differences are however rather small and will likely not lead to any significant differences in the cut efficiencies.

Regarding the lepton p_T , the small difference that appears is between the L and R cases rather than between SUSY and XQ: all the (600, 10)R scenarios exhibit somewhat harder $p_T(l)$ than the (600, 10)L scenarios. This comes from the fact that the top polarisation influences the p_T of the top decay products. These features persist for smaller top-partner–DM mass difference, see Fig. 4.

Polarisation effects in stop decays were studied in detail in [41–51]. Sizeable effects were found in kinematic distributions of the final-state leptons and b -quarks, and in particular in their angular correlations. While this might help to constrain the relevant mixing angles in precision studies of a positive signal [44, 45, 47–50] and possibly to characterise the spin of the top-partner mediators and of the DM states through the structure of their coupling [43, 45, 46], as we will see, the current experimental analyses are not very sensitive to these effects.

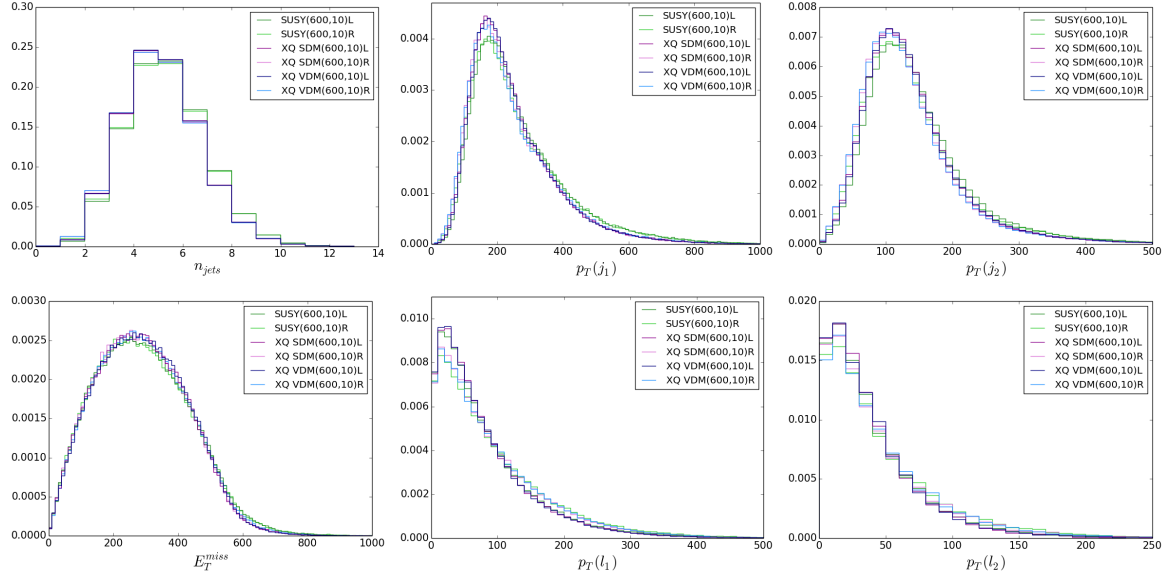


Figure 3. Differential distributions (normalized to one) of jet multiplicity n_{jets} , transverse momentum of the leading and sub-leading jet $p_T(j_1)$ and $p_T(j_2)$, missing transverse energy E_T^{miss} , and p_T of the leading and sub-leading lepton $p_T(l_1)$ and $p_T(l_2)$ for the mass combination (600, 10).

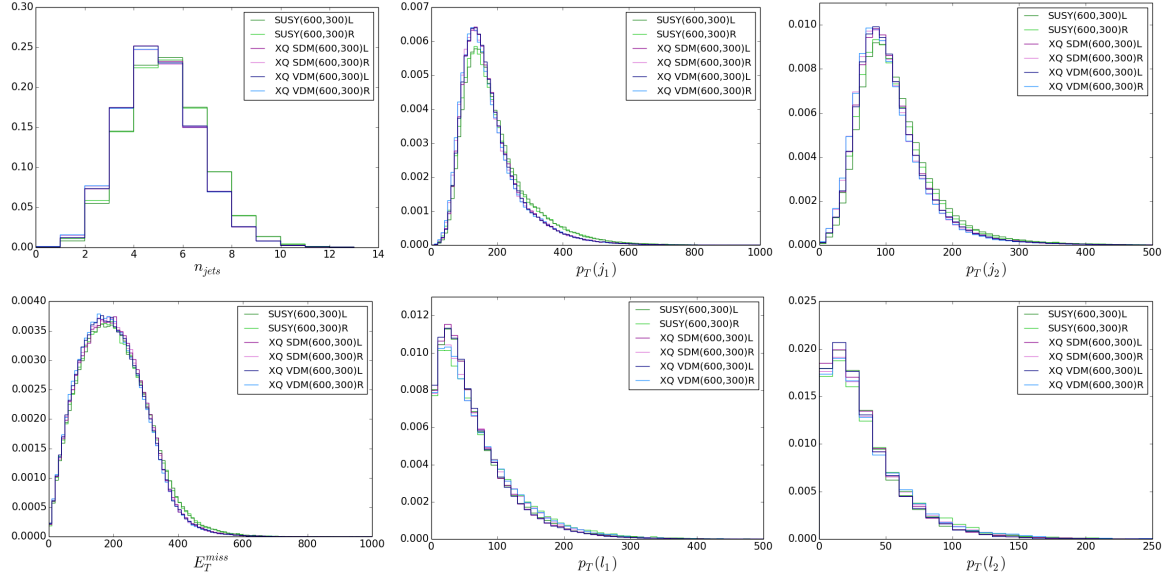


Figure 4. Same as Fig. 3 but for the (600, 300) mass combination.

4 Effects in existing 8 TeV analyses

Let us now analyse how the cut acceptances of existing 8 TeV analyses compare for the SUSY and XQ scenarios. To this end, we consider the following ATLAS and CMS analyses implemented in CHECKMATE [24] or the MADANALYSIS 5 Public Analysis Database (MA5 PAD) [26]:

- Fully hadronic stop search: ATLAS-CONF-2013-024 [19] implemented in CHECKMATE, see Section 4.1
- Stop searches in the single lepton mode from ATLAS [20] (CHECKMATE) and CMS [21] (MA5 PAD, recast code [76]), see Section 4.2
- The stop search with 2 leptons from ATLAS [22] implemented in CHECKMATE, see Section 4.3
- The generic gluino/squark search in the 2–6 jets plus missing energy channel from ATLAS [23] (MA5 PAD, recast code [77]), see Section 4.4

4.1 Fully hadronic stop search

The ATLAS analysis [19] implemented in CHECKMATE targets stop-pair production followed by stop decays into a top quark and the lightest neutralino, $pp \rightarrow \tilde{t}_1 \tilde{t}_1^* \rightarrow t \bar{t} \tilde{\chi}_1^0 \tilde{\chi}_1^0$ in the fully-hadronic top final state, $t \rightarrow bW \rightarrow bq\bar{q}$. The search is thus conducted in events with large missing transverse momentum and six or more jets, of which ≥ 2 must have been b -tagged. The two leading jets are required to have $p_T > 80$ GeV with the remaining jets having $p_T > 35$ GeV. Pre-selected electrons or muons, as well as taus are vetoed. Further requirements are imposed on azimuthal angle ($\Delta\phi$) and transverse mass (m_T) variables and on two 3-jet systems. Then three overlapping signal regions (SRs) are defined by requirements on E_T^{miss} , SR1: $E_T^{\text{miss}} \geq 200$ GeV, SR2: $E_T^{\text{miss}} \geq 300$ GeV and SR3: $E_T^{\text{miss}} \geq 350$ GeV.⁶

The effect of the various cuts is illustrated in Table 2 for the example of Point (600,10)L. We observe that most preselection cuts have very similar efficiencies⁷

⁶We note that the conference note [19] was superseded by the paper publication [78], which has six SRs targeting the $\tilde{t}_1 \rightarrow t \tilde{\chi}_1^0$ decay instead of three. Four of these, SRA1–4, are for “fully resolved” events with ≥ 6 jets and a stacked E_T^{miss} cut of 150, 250, 300 and 350 GeV. This is similar to the conference note. Two more SRs, SRB1–2, are for “partially resolved” events with 4 or 5 jets and higher E_T^{miss} , designed to target high stop masses. Moreover, the paper considers three SRs, SRC1–3, optimized for stop decays into charginos. The limit is then set from a combination of SRA+B or SRA+C. Since this cannot be reproduced without a prescription of how to combine the SRs, we keep using the CHECKMATE implementation of the conference note to test the efficiencies of the hadronic stop search for our benchmark points. This is also justified by the fact that we are not primarily interested in the absolute limit but in potential differences in selection efficiencies between scalar and fermionic top partners.

⁷Here and in the following, we use the term “efficiency” for the percentage of events remaining after one or more cuts. Strictly speaking this is the quantity acceptance \times efficiency, $A\epsilon$.

	SUSY	XQ-SDM	XQ-VDM
Initial no. of events	200000	200000	200000
$E_T^{\text{miss}} > 80$ GeV (Trigger)	187834 (-6.08 %)	187872 (-6.06 %)	188358 (-5.82 %)
muon veto ($p_T > 10$ GeV)	154643 (-17.67 %)	153946 (-18.06 %)	154710 (-17.86 %)
electron veto ($p_T > 10$ GeV)	123420 (-20.19 %)	122439 (-20.47 %)	123247 (-20.34 %)
$E_T^{\text{miss}} > 130$ GeV	113638 (-7.93 %)	112808 (-7.87 %)	113620 (-7.81 %)
≥ 6 jets, $p_T > 80, 80, 35$ GeV	33044 (-70.92 %)	27987 (-75.19 %)	28285 (-75.11 %)
reconstr. $E_T^{\text{miss, track}} > 30$ GeV	32564 (-1.45 %)	27563 (-1.51 %)	27901 (-1.36 %)
$\Delta\phi(E_T^{\text{miss}}, E_T^{\text{miss, track}}) < \pi/3$	31200 (-4.19 %)	26583 (-3.56 %)	26939 (-3.45 %)
$\Delta\phi(E_T^{\text{miss}}, 3 \text{ hdst jets}) > 0.2\pi$	26276 (-15.78 %)	22795 (-14.25 %)	23129 (-14.14 %)
tau veto	22880 (-12.92 %)	19967 (-12.41 %)	20354 (-12.00 %)
$2 b$ jets	9668 (-57.74 %)	8510 (-57.38 %)	8660 (-57.45 %)
$m_T(b \text{ jets}) > 175$ GeV	7202 (-25.51 %)	6447 (-24.24 %)	6579 (-24.03 %)
3 closest jets 80–270 GeV	6437 (-10.62 %)	5877 (-8.84 %)	5929 (-9.88 %)
same for second closest jets	3272 (-49.17 %)	3186 (-45.79 %)	3351 (-43.48 %)
$E_T^{\text{miss}} \geq 150$ GeV	3230 (-1.28 %)	3156 (-0.94 %)	3312 (-1.16 %)
$E_T^{\text{miss}} \geq 200$ GeV (SR1)	3067 (-5.05 %)	3000 (-4.94 %)	3161 (-4.56 %)
$E_T^{\text{miss}} \geq 250$ GeV	2795 (-8.87 %)	2732 (-8.93 %)	2867 (-9.30 %)
$E_T^{\text{miss}} \geq 300$ GeV (SR2)	2413 (-13.67 %)	2373 (-13.14 %)	2490 (-13.15 %)
$E_T^{\text{miss}} \geq 350$ GeV (SR3)	1948 (-19.27 %)	1926 (-18.84 %)	2010 (-19.28 %)

Table 2. Cut-flow of the hadronic stop analysis of ATLAS for Point (600, 10)L, derived with CHECKMATE.

when comparing SUSY and XQ cases. Small differences, of the level of few percent, occur only in the requirement of at least six jets (cf. Fig. 3) and the condition on “3 closest jets” and “second closest jets”, but these differences tend to compensate each other. Finally, the effect of the E_T^{miss} cuts that define the three SRs is almost the same for the SUSY and XQ scenarios. Consequently, the final numbers of events in each of the SRs agree within $\lesssim 5\%$ for the SUSY and XQ scenarios.

The total efficiencies in the three SRs, cross-section excluded at 95% CL and corresponding top-partner mass limits in GeV are compared in Table 3 for all four benchmark scenarios.⁸ We see that for a specific mass combination, the total efficiencies and hence the upper limit on the cross-section are very similar for the SUSY and XQ hypotheses. The derived lower limit on the top-partner mass of course depends on the input cross-section (whether it is assumed SUSY-like or XQ-like), and is thus higher for the XQ interpretation than for the SUSY interpretation. However, the differences in the mass limits arising from applying SUSY, XQ-SDM or XQ-VDM efficiencies are generally small. Indeed for the (600, 10) scenarios, i.e. large mass splitting, they are only 2–4 GeV, which is totally negligible. For smaller mass splittings, represented by the (600, 300) scenarios, they reach about 10–20 GeV, which is still negligible. Finally, note that the effect on the mass limit from considering L vs.

⁸Given the upper limit on the cross-section together with the cross-section prediction as a function of the top-partner mass one can estimate the 95% CL mass limit under the assumption that the efficiency is flat. While this kind of extrapolation is not a substitute for determining the true limit through a scan over the masses, it does give an indication of i) the impact of the differences in the excluded cross-section and ii) the higher reach in XQ as compared to SUSY. As we will see, this extrapolation works reasonably well for the stop searches but not for analyses that involve cuts which are directly sensitive to the overall mass scale.

	Point (600, 10)L			Point (600, 10)R		
	SUSY	XQ-SDM	XQ-VDM	SUSY	XQ-SDM	XQ-VDM
eff. SR1	0.015	0.015	0.016	0.014	0.015	0.014
eff. SR2	0.012	0.012	0.012	0.011	0.012	0.011
eff. SR3*	0.0097	0.0096	0.010	0.0092	0.0095	0.0094
excl. XS [pb]	0.0196	0.0199	0.0189	0.0209	0.0201	0.0205
mass limit/SUSY XS	619	618	622	613	617	615
mass limit/XQ XS	805	803	808	798	802	800
1 – CLs	0.98	1	1	0.97	1	1

	Point (600, 300)L			Point (600, 300)R		
	SUSY	XQ-SDM	XQ-VDM	SUSY	XQ-SDM	XQ-VDM
eff. SR1*	0.0074	0.0064	0.0062	0.0066	0.0060	0.0053
eff. SR2	0.0039	0.0032	0.0031	0.0035	0.0032	0.0026
eff. SR3	0.0022	0.0016	0.0017	0.0018	0.0016	0.0013
excl. XS [pb]	0.0647	0.0759	0.0772	0.0726	0.0805	0.0910
mass limit/SUSY XS	522	510	509	514	506	497
mass limit/XQ XS	687	671	670	676	666	655
1 – CLs	0.59	1	1	0.54	1	1

Table 3. Efficiencies in the three SRs, cross-section (XS) excluded at 95% CL, corresponding extrapolated top-partner mass limits in GeV, and CLs exclusion value from the hadronic stop analysis of ATLAS derived with CHECKMATE. “mass limit/SUSY XS” means that the excluded XS is translated to a mass limit using the SUSY production cross-section from Fig. 2, while “mass limit/XQ XS” means the limit is estimated using the XQ cross-section. The exclusion CL is obtained considering the corresponding cross-sections at 600 GeV, $\sigma(\tilde{t}_1\tilde{t}_1^*) = 0.024$ pb for stop production and $\sigma(T\bar{T}) = 0.167$ pb for XQ production. The most sensitive SR used for the limit setting is marked with a star.

R polarised tops is of comparable size.

4.2 Stop search in the single lepton final state

Stops are also searched for in final states with a single lepton, jets and E_T^{miss} , arising from one W decaying leptonically while the other one decays hadronically. The ATLAS analysis [20] for this channel is implemented in CHECKMATE, while the (cut-based version of) the corresponding CMS analysis [21] is implemented in the MA5 PAD.

In the CMS analysis [21], events are required to contain one isolated electron (muon) with $p_T > 30$ (25) GeV, no additional isolated track or hadronic τ candidate, at least four jets with $p_T > 30$ GeV at least one of which must be b -tagged, $E_T^{\text{miss}} > 100$ GeV and $M_T > 120$ GeV. The analysis further makes use of the quantity M_{T2}^W , a hadronic top χ^2 ensuring that three of the jets in the event be consistent with the $t \rightarrow bW \rightarrow bq\bar{q}$ decay, and the topological variable $\Delta\phi(E_T^{\text{miss}}, \text{jet})$. Various signal regions are defined targeting $\tilde{t}_1 \rightarrow t\tilde{\chi}_1^0$ or $\tilde{t}_1 \rightarrow b\tilde{\chi}_1^+$ decays with small or large mass differences between the stop and the neutralino or chargino.

As an illustrative example, we show in Table 4 the cut-flow for the “ $\tilde{t}_1 \rightarrow t\tilde{\chi}_1^0$, high ΔM , $E_T^{\text{miss}} > 300$ GeV” signal region for Point (600, 10)R, which is the most sensitive SR for this benchmark. The only noticeable difference, though hardly of

	SUSY	XQ-SDM	XQ-VDM
Initial no. of events	200000	200000	200000
≥ 1 candidate lepton	51097 (-74.45 %)	50700 (-74.65 %)	50417 (-74.79 %)
≥ 4 central jets	23737 (-53.55 %)	21333 (-57.92 %)	20997 (-58.35 %)
$E_T^{\text{miss}} > 50$ GeV	23203 (-2.25 %)	20848 (-2.27 %)	20548 (-2.14 %)
$E_T^{\text{miss}} > 100$ GeV	21640 (-6.74 %)	19393 (-6.98 %)	19206 (-6.53 %)
≥ 1 b -tagged jet	18339 (-15.25 %)	16643 (-14.18 %)	16512 (-14.03 %)
isol lepton and track veto	17370 (-5.28 %)	15892 (-4.51 %)	15750 (-4.61 %)
hadronic tau veto	17061 (-1.78 %)	15646 (-1.55 %)	15487 (-1.67 %)
$M_T > 120$ GeV	13811 (-19.05 %)	12788 (-18.27 %)	12691 (-18.05 %)
$\Delta\phi(E_T^{\text{miss}}, j1 \text{ or } j2) > 0.8$	12006 (-13.07 %)	11251 (-12.02 %)	11164 (-12.03 %)
$\chi^2 < 5$	7079 (-41.04 %)	6771 (-39.82 %)	6750 (-39.54 %)
$E_T^{\text{miss}} > 300$ GeV	4138 (-41.55 %)	3820 (-43.58 %)	3929 (-41.79 %)
$M_{T2}^W > 200$ GeV	3030 (-26.78 %)	2830 (-25.92 %)	2851 (-27.44 %)

Table 4. Cut-flow for the “ $\tilde{t}_1 \rightarrow t\tilde{\chi}_1^0$, high ΔM , $E_T^{\text{miss}} > 300$ GeV” signal region (denoted SR-A) of the CMS stop search in the 1-lepton channel for Point (600,10)R, derived with the MADANALYSIS 5 recast code [76]. Note that the event weighting to account for trigger and lepton identification efficiencies and for initial-state radiation effects is not included in this cut-flow. More details about these aspects and their implementation of the recast code can be found in the original references [21] and [76].

	Point (600, 10)L			Point (600, 10)R		
	SUSY	XQ-SDM	XQ-VDM	SUSY	XQ-SDM	XQ-VDM
eff. SR-A	0.0108	0.0109	0.0111	0.0108*	0.0106*	0.0107*
eff. SR-B	0.0181*	0.0176*	0.0184*	0.0154	0.0152	0.0153
excl. XS [pb]	0.0169	0.0173	0.0166	0.0210	0.0213	0.0211
mass limit/SUSY XS	631	629	633	613	611	612
mass limit/XQ XS	820	818	822	798	796	797
1 – CLs	0.99	1	1	0.97	1	1

	Point (600, 300)L			Point (600, 300)R		
	SUSY	XQ-SDM	XQ-VDM	SUSY	XQ-SDM	XQ-VDM
eff. SR-A	0.00360	0.00366	0.00346	0.00340	0.00321	0.00315
eff. SR-B	0.00748*	0.00685*	0.00632*	0.00597*	0.00570*	0.00536*
excl. XS [pb]	0.0399	0.0448	0.0480	0.0507	0.0530	0.0563
mass limit/SUSY XS	560	551	546	541	538	533
mass limit/XQ XS	733	722	715	710	706	700
1 – CLs	0.81	1	1	0.72	1	1

Table 5. Efficiencies for the “ $\tilde{t}_1 \rightarrow t\tilde{\chi}_1^0$, high ΔM , $E_T^{\text{miss}} > 300$ GeV” (denoted SR-A) and “ $\tilde{t}_1 \rightarrow b\tilde{\chi}_1^+$, high ΔM , $E_T^{\text{miss}} > 250$ GeV” (denoted SR-B) signal regions, cross-sections excluded at 95% CL, corresponding extrapolated top-partner mass limits in GeV, and CLs exclusion value from the 1-lepton stop analysis of CMS, derived with the MADANALYSIS 5 recast code [76]. The most sensitive SR used for the limit setting is indicated by a star.

the level of 5% in the cut efficiency, arises from the requirement of at least four jets. All other cuts have again almost the same effects on the SUSY and XQ models. Altogether, starting from the same number of events, we end up with slightly more SUSY than XQ events in this SR, but this difference is only 6–7%.

Table 5 summarises the total efficiencies in the two most important SRs of this analysis, the cross-sections excluded at 95% CL and the corresponding top-partner

mass limits in GeV for all four benchmark scenarios. Note that, for large mass splitting, the SRs “ $\tilde{t}_1 \rightarrow b\tilde{\chi}_1^+$, high ΔM , $E_T^{\text{miss}} > 250$ GeV” (here denoted as SR-B) which is optimized for $\tilde{t}_1 \rightarrow b\tilde{\chi}_1^+$ decays and “ $\tilde{t}_1 \rightarrow t\tilde{\chi}_1^0$, high ΔM , $E_T^{\text{miss}} > 300$ GeV” (denoted SR-A) optimized for $\tilde{t}_1 \rightarrow t\tilde{\chi}_1^0$ have very similar sensitivities. In fact we observe that the most sensitive SR depends on the top polarisation. Events with left polarised tops are more likely to pass the additional requirement of SR-B on the leading b -jet, $p_T > 100$ GeV. Concretely, in the SUSY scenario the expected upper limits are 0.0290 pb in SR-A versus 0.0251 pb in SR-B for (600,10)L and 0.0291 pb vs. 0.0295 pb for (600,10)R. CMS has observed a small underfluctuation in both these SRs: 2 observed events vs. 4.7 ± 1.4 expected in SR-A and 5 observed events vs. 9.9 ± 2.7 expected in SR-B. Overall the observed cross-section limit is somewhat lower in the left-polarised scenario. An analogous observation holds for the XQ scenarios; the differences between SUSY and XQ scenarios are negligible.

Finally, for smaller mass gaps, SR-B is more sensitive in all considered scenarios and we observe differences at the level of 10–15% in the total signal selection efficiencies, which translate into up to about 20% differences in the excluded cross-sections, or $\lesssim 5\%$ in the estimated mass limits. The uncertainty from considering scenarios that lead to left or right polarised tops is of similar magnitude. The latter is consistent with the observation in [21] that the limits on the \tilde{t}_1 and $\tilde{\chi}_1^0$ masses vary by ± 10 –20 GeV depending on the top-quark polarisation; the polarisation dependence in the $\tilde{t}_1 \rightarrow b\tilde{\chi}_1^+$ channel can be somewhat larger.

The corresponding ATLAS search [20] for this channel is implemented in CHECKMATE. Here, the signal selection requires a least one “baseline” lepton with $p_T > 10$ GeV, which is later tightened to exactly one isolated lepton with $p_T > 25$ GeV.⁹ Events containing additional baseline leptons are rejected. The analysis comprises 15 non-exclusive SRs, 4 of which target $\tilde{t}_1 \rightarrow t\tilde{\chi}_1^0$ (labelled ‘tN_’), 9 target $\tilde{t}_1 \rightarrow b\tilde{\chi}_1^+$ (labelled ‘bC_’), and the last 2 target 3-body and mixed decays. A minimum number of jets ranging between 2 and 4 is required depending on the SR, together with b -tagging requirements and an E_T^{miss} cut of at least 100 GeV. As for the CMS analysis, a number of kinematic variables (m_T , am_{T2} , $\Delta\phi(E_T^{\text{miss}}, \vec{p}_T(\text{jet}))$, etc.) are exploited for reducing the background. The relevant SRs for our benchmark points are tN_med, bCd_high and bCd_bulk.¹⁰ Of course, for the limit setting only the most sensitive one is used. A partial cut-flow example is given in Table 6 for Point (600, 10)R. The results for all four benchmark points are summarised in Table 7.

As in the CMS analysis, we observe very similar sensitivities in several signal regions, and it depends on details of the scenario which SR turns out as the best

⁹Except for the SR with soft-lepton selections which employ a $p_T > 6(7)$ GeV requirement for muons (electrons).

¹⁰Note that the ATLAS search has a dedicated SR to target boosted final states, tN_boost. This SR is not considered here, as the relevant “topness” variable is not implemented in CHECKMATE.

	SUSY	XQ-SDM	XQ-VDM
Initial no. of events	200000	200000	200000
Trigger	158881 (-20.56 %)	158929 (-20.54 %)	160073 (-19.96 %)
DQ	154759 (-2.59 %)	155073 (-2.43 %)	156148 (-2.45 %)
1 baseline electron	30142 (-80.52 %)	29980 (-80.67 %)	30019 (-80.78 %)
1 signal electron	22342 (-25.88 %)	22177 (-26.03 %)	22169 (-26.15 %)
≥ 3 jets $p_T \geq 25$ GeV	19865 (-11.09 %)	19241 (-13.24 %)	19262 (-13.11 %)
≥ 4 jets $p_T \geq 25$ GeV	14458 (-27.22 %)	13275 (-31.01 %)	13355 (-30.67 %)
...			
tN_med e	1892 (-86.91 %)	1951 (-85.30 %)	1987 (-85.12 %)
bCd_high1 e	1792 (-87.61 %)	1651 (-87.56 %)	1748 (-86.91 %)
bCd_bulk e	4359 (-69.85 %)	4180 (-68.51 %)	4262 (-68.09 %)
1 baseline μ	27993 (-81.91 %)	28381 (-81.70 %)	28119 (-81.99 %)
1 signal μ	23123 (-17.40 %)	23383 (-17.61 %)	23088 (-17.89 %)
≥ 3 jets $p_T \geq 25$ GeV	20695 (-10.50 %)	20624 (-11.80 %)	20302 (-12.07 %)
≥ 4 jets $p_T \geq 25$ GeV	15197 (-26.57 %)	14448 (-29.95 %)	14163 (-30.24 %)
...			
tN_med μ	2108 (-86.13 %)	1970 (-86.36 %)	1977 (-86.04 %)
bCd_high1 μ	1790 (-88.22 %)	1821 (-87.40 %)	1747 (-87.67 %)
bCd_bulk μ	4582 (-69.85 %)	4415 (-69.44 %)	4340 (-69.36 %)

Table 6. Partial cut-flows for the ATLAS stop search in the 1-lepton channel for Point (600,10)R, derived with CHECKMATE. Shown are the effects of the preselection cuts and the final numbers of events in specific signal regions. The cut-flows are given separately for electrons and muons.

	Point (600,10)L			Point (600,10)R		
	SUSY	XQ-SDM	XQ-VDM	SUSY	XQ-SDM	XQ-VDM
eff. bCd_bulk_d	0.0298*	0.0287	0.0297	0.0278*	0.0264*	0.0270*
eff. bCd_high1	0.0208	0.0204*	0.0210*	0.0179	0.0174	0.0175
excl. XS [pb]	0.0250	0.0335	0.0324	0.0267	0.0281	0.0274
mass limit/SUSY XS	598	574	577	593	588	590
mass limit/XQ XS	780	750	754	773	768	770
1 - CLs	0.94	1	1	0.93	1	1

	Point (600,300)L			Point (600,300)R		
	SUSY	XQ-SDM	XQ-VDM	SUSY	XQ-SDM	XQ-VDM
eff. bCd_high1	0.00919*	0.00810*	0.00761*	0.00777	0.00691	0.00638
eff. tN_med	0.00927	0.00869	0.00836	0.00877*	0.00862*	0.00775*
excl. XS [pb]	0.0742	0.0845	0.0898	0.0509	0.0517	0.0579
mass limit/SUSY XS	512	502	498	541	540	531
mass limit/XQ XS	673	661	656	709	708	697
1 - CLs	0.35	1	1	0.69	1	1

Table 7. Efficiencies for selected SRs, cross-sections excluded at 95% CL, corresponding extrapolated top-partner mass limits in GeV, and CLs exclusion values for the ATLAS stop search in the 1-lepton channel, derived with CHECKMATE. The most sensitive SR used for the limit setting is indicated by a star.

one. It should be noted here that small differences in selection efficiencies can have a considerable impact on the observed limit if they yield different SRs as the most sensitive one. In particular, ATLAS has observed more events than expected in SR bCd_high1 (16 observed events vs. 11 ± 1.5 expected). Consequently, limits obtained from this SR are weaker than those using tN_med (12 observed vs. 13 ± 2.2 expected)

or `bCd_bulk_d` (29 observed vs. 26.5 ± 2.6 expected). This is relevant, for example, for Point (600, 10)L. Nonetheless, the differences when comparing SUSY, XQ-SDM and XQ-VDM cases remain small, in particular always well below the 20–30% estimated systematic uncertainty inherent to recasting with fast simulation tools. It is also worth pointing out that, in contrast to its CMS counterpart, this ATLAS analysis tends to give stronger limits for R than for L scenarios. The effect is more pronounced for smaller mass differences, in agreement with Fig. 24 in [20]. Overall, the sensitivity to polarisation effects, while larger than for the CMS analysis, remains small.

4.3 Stop search in the 2-leptons final state

Let us next discuss the 2-lepton final state considered in the ATLAS analysis [22]. This analysis searches for direct stop-pair production with $\tilde{t}_1 \rightarrow b\tilde{\chi}_1^+ \rightarrow bW^{(*)}\tilde{\chi}_1^0$ or $\tilde{t}_1 \rightarrow t\tilde{\chi}_1^0 \rightarrow bW\tilde{\chi}_1^0$, targeting leptonic W decays. Events are required to have exactly two oppositely charged signal leptons (electrons, muons or one of each, defining same flavour (SF) and different-flavour (DF) selections). At least one of these electrons or muons must have $p_T > 25$ GeV and $m_{\ell\ell} > 20$ GeV. Events with a third preselected electron or muon are rejected. The analysis is subdivided into a “leptonic mT2” and “hadronic mT2” analysis, as well a multivariate analysis (MVA), which cannot be reproduced with our simulation frameworks. The “leptonic mT2” (4 SRs) and “hadronic mT2” (1 SR) analyses respectively use m_{T2} and $m_{T2}^{b\text{-jet}}$ as the key discriminating variable. Other kinematic variables used include $\Delta\phi_j$ ($\Delta\phi_\ell$), the azimuthal angular distance between the p_T^{miss} vector and the direction of the closest jet (highest p_T lepton).

The “leptonic mT2” analysis has 4 overlapping SRs defined by $m_{T2} > 90, 100, 110$ and 120 GeV. From these, seven statistically independent SRs denoted S1–S7 are defined in the (jet selections, m_{T2}) plane, where ‘jet selections’ refers to the number of jets with a certain minimum p_T , see Fig. 13 in [22]. The most sensitive one for our benchmark points is S5, which has $m_{T2} > 120$ GeV and at least two jets with $p_T(\text{jet1}) > 100$ GeV and $p_T(\text{jet2}) > 50$ GeV.

Table 8 shows a cut-flow example for the SF selection for Point (600, 10)R, as well as an abbreviated version for the DF selection. Note that the leptonic W decay was enforced in PYTHIA to increase statistics. The SF selection gives less events than the DF one because the Z veto removes about 20% of events in the former but none in the latter. The combined count for SR S5 is given as the last line in the table. As was already the case for the other analyses, no significant differences occur at any particular step of the cut-flow. At the end we are left with the marginal difference of 4% more XQ than SUSY events in a total selection efficiency of barely 3 permil (when considering events where the W is allowed to decay to anything).

The picture is similar for Point (600, 10)L, for which the cut-flow is given in Table 9. Noteworthy is the fact that the initial difference in Points (600, 10)R and (600, 10)L from the 2 lepton selection (the first cut) is inverted by the last cut, so

	SUSY	XQ-SDM	XQ-VDM
Initial no. of events	200000	200000	200000
2 leptons, $p_T > 10$ GeV	63129 (-68.44 %)	63877 (-68.06 %)	63604 (-68.20 %)
same flavour	31464 (-50.16 %)	32040 (-49.84 %)	31643 (-50.25 %)
isolation	28096 (-10.70 %)	28538 (-10.93 %)	28234 (-10.77 %)
opposite sign	27961 (-0.48 %)	28402 (-0.48 %)	28078 (-0.55 %)
$m_{\ell\ell} > 20$ GeV	27457 (-1.80 %)	27874 (-1.86 %)	27586 (-1.75 %)
$p_T(\ell) > 25$ GeV	26505 (-3.47 %)	26948 (-3.32 %)	26625 (-3.48 %)
Z veto	21448 (-19.08 %)	21682 (-19.54 %)	21374 (-19.72 %)
$\Delta\phi_j > 1$	12664 (-40.95 %)	13463 (-37.91 %)	13375 (-37.42 %)
$\Delta\phi_b < 1.5$	11779 (-6.99 %)	12638 (-6.13 %)	12460 (-6.84 %)
$m_{T2} > 120$ GeV	4824 (-59.05 %)	5441 (-56.95 %)	5368 (-56.92 %)
S5 – SF (2 jets, $p_T > 100, 50$ GeV)	2378 (-50.70 %)	2621 (-51.83 %)	2446 (-54.43 %)
different flavour	31665 (-49.84 %)	31837 (-50.16 %)	31961 (-49.75 %)
...			
$m_{T2} > 120$ GeV	5955 (-59.74 %)	6515 (-58.31 %)	6697 (-57.45 %)
S5 – DF (2 jets, $p_T > 100, 50$ GeV)	3032 (-49.08 %)	3013 (-53.75 %)	3030 (-54.76 %)
S5 – SF+DF	5410	5634	5476

Table 8. Cut-flow example for the ATLAS stop search in the 2-lepton channel for Point (600,10)R, derived with CHECKMATE. Here, the leptonic W decay was enforced to enhance statistics.

	SUSY	XQ-SDM	XQ-VDM
Initial no. of events	200000	200000	200000
2 leptons, $p_T > 10$ GeV	60379 (-69.81 %)	61193 (-69.40 %)	60812 (-69.59 %)
same flavour	30109 (-50.13 %)	30508 (-50.14 %)	30419 (-49.98 %)
isolation	26759 (-11.13 %)	27108 (-11.14 %)	27066 (-11.02 %)
opposite sign	26660 (-0.37 %)	26994 (-0.42 %)	26987 (-0.29 %)
$m_{\ell\ell} > 20$ GeV	26043 (-2.31 %)	26364 (-2.33 %)	26381 (-2.25 %)
$p_T(\ell) > 25$ GeV	25062 (-3.77 %)	25251 (-4.22 %)	25345 (-3.93 %)
Z veto	19570 (-21.91 %)	19765 (-21.73 %)	19642 (-22.50 %)
$\Delta\phi_j > 1$	11797 (-39.72 %)	12485 (-36.83 %)	12522 (-36.25 %)
$\Delta\phi_b < 1.5$	11270 (-4.47 %)	11943 (-4.34 %)	12035 (-3.89 %)
$m_{T2} > 120$ GeV	4390 (-61.05 %)	4785 (-59.93 %)	4815 (-59.99 %)
S5 – SF (2 jets, $p_T > 100, 50$ GeV)	2711 (-38.25 %)	2803 (-41.42 %)	2841 (-41.00 %)
different flavour	30270 (-49.87 %)	30685 (-49.86 %)	30393 (-50.02 %)
...			
$\Delta\phi_j > 1$	15273 (-38.59 %)	16117 (-36.31 %)	15896 (-36.21 %)
$\Delta\phi_b < 1.5$	14683 (-3.86 %)	15505 (-3.80 %)	15260 (-4.00 %)
$m_{T2} > 120$ GeV	5581 (-61.99 %)	6149 (-60.34 %)	5985 (-60.78 %)
S5 – DF (2 jets, $p_T > 100, 50$ GeV)	3524 (-36.86 %)	3562 (-42.07 %)	3503 (-41.47 %)
S5 – SF+DF	6235	6365	6344

Table 9. Cut-flow example for the ATLAS stop search in the 2-lepton channel for Point (600,10)L, derived with CHECKMATE. To be compared with Table 8. W s were again forced to decay leptonically to enhance statistics.

that in the final SR there remain more events for (600,10)L than for (600,10)R. This is a consequence of the dependence on the top polarisation already noted in the parton-level plots in Figs. 3 and 4.

Either way, as can be seen from Table 10, there is again no significant difference in the total efficiencies and excluded cross-sections between SUSY, XQ-SDM and XQ-VDM scenarios.

	Point (600, 10)L			Point (600, 10)R		
	SUSY	XQ-SDM	XQ-VDM	SUSY	XQ-SDM	XQ-VDM
efficiency	0.00314	0.00334	0.00323	0.00276	0.00285	0.00286
excl. XS [pb]	0.0470	0.0443	0.0455	0.0535	0.0520	0.0518
mass limit/SUSY XS	547	552	550	537	539	540
mass limit/XQ XS	717	723	720	705	707	708
1 – CLs	0.79	1	1	0.74	1	1

	Point (600, 300)L			Point (600, 300)R		
	SUSY	XQ-SDM	XQ-VDM	SUSY	XQ-SDM	XQ-VDM
efficiency	0.00134	0.001425	0.00138	0.00111	0.00118	0.00100
excl. XS [pb]	0.109	0.104	0.108	0.133	0.125	0.148
mass limit/SUSY XS	484	487	484	469	473	462
mass limit/XQ XS	638	642	639	620	626	611
1 – CLs	0.49	1	1	0.43	1	1

Table 10. Efficiencies, cross-sections excluded at 95% CL, corresponding extrapolated top-partner mass limits in GeV, and CLs exclusion value for the ATLAS stop search in the 2-lepton channel, derived with CHECKMATE. All numbers correspond to the most sensitive signal region, SR5.

4.4 Gluino/squark search in the 2–6 jets final state

For completeness, we also include a generic SUSY search (nominally for squarks and gluinos) in final states containing high- p_T jets, missing transverse momentum and no electrons or muons in our analysis. Concretely, we here consider the ATLAS analysis [23] via the MADANALYSIS 5 recast code [77]. (A CHECKMATE implementation of the same analysis was done in [79] and will be used in Appendix A). Our original purpose was to compare the performance of the hadronic stop analysis to that of a multi-jet analysis which was not optimized for the $t\bar{t} + E_T^{\text{miss}}$ signature. But, as we will see, the effective mass M_{eff} variable employed in the generic gluino/squark search offers a useful complementary probe.

Regarding the signal selection, the ATLAS analysis [23] comprises 15 inclusive SRs characterized by increasing minimum jet multiplicity, N_j , from two to six jets. Hard cuts are placed on missing energy and the p_T of the two leading jets: $E_T^{\text{miss}} > 160$ GeV, $p_T(j_1) > 130$ GeV and $p_T(j_2) > 60$ GeV. For the other jets, $p_T > 60$ or 40 GeV is required depending on the SR. In all cases, events are discarded if they contain electrons or muons with $p_T > 10$ GeV. Depending on N_j , additional requirements are placed on the minimum azimuthal separation between any of the jets and the E_T^{miss} , $\Delta\phi(\text{jet}, E_T^{\text{miss}})$, as well as on $E_T^{\text{miss}}/\sqrt{H_T}$ or $E_T^{\text{miss}}/M_{\text{eff}}(N_j)$. Finally, a cut is placed on $M_{\text{eff}}(\text{incl.})$, which sums over all jets with $p_T > 40$ GeV and E_T^{miss} . A cut-flow example is shown in Table 11 for Point (600,10)R for a SR with 4 jets (SR 4j1). Note that, starting from 200K events, we end up with about 15% (11%) more SUSY than XQ-SDM (XQ-VDM) events in this SR. The reason for this is that the cuts on $p_T(j)$ and M_{eff} remove somewhat more XQ than SUSY events, as expected from the distributions in Fig. 3.

	SUSY	XQ-SDM	XQ-VDM
Initial no. of events	200000	200000	200000
$E_T^{\text{miss}} > 160$ GeV	158489 (-20.76%)	158497 (-20.75%)	159683 (-20.16%)
$N_j > 1$	150908 (-4.78%)	150121 (-5.28%)	151311 (-5.24%)
lepton veto	100139 (-33.64%)	100462 (-33.08%)	101404 (-32.98%)
$p_T(j_1) > 130$ GeV	62585 (-37.50%)	58754 (-41.52%)	59482 (-41.34%)
$p_T(j_2) > 60$ GeV	62045 (-0.86%)	58188 (-0.96%)	58886 (-1.00%)
$p_T(j_3) > 60$ GeV	56729 (-8.57%)	52649 (-9.52%)	53312 (-9.47%)
$p_T(j_4) > 60$ GeV	39150 (-30.99%)	34856 (-33.80%)	35258 (-33.86%)
$\Delta\phi(j_1, E_T^{\text{miss}}) > 0.4$	38811 (-0.87%)	34616 (-0.69%)	35000 (-0.73%)
$\Delta\phi(j_2, E_T^{\text{miss}}) > 0.4$	37199 (-4.15%)	33304 (-3.79%)	33635 (-3.90%)
$\Delta\phi(j_3, E_T^{\text{miss}}) > 0.4$	35447 (-4.71%)	31870 (-4.31%)	32211 (-4.23%)
$\Delta\phi(j_4, E_T^{\text{miss}}) > 0.2$	34535 (-2.57%)	31064 (-2.53%)	31435 (-2.41%)
$E_T^{\text{miss}}/\sqrt{H_T} > 10$	25451 (-26.30%)	23522 (-24.28%)	24004 (-23.64%)
$M_{\text{eff}}(\text{incl.}) > 1$ TeV	17695 (-30.47%)	15062 (-35.97%)	15714 (-34.54%)

Table 11. Cut-flow for the 4j1 SR of the ATLAS gluino and squark search in the 2–6 jets channel for Point (600, 10)R, derived with the MADANALYSIS 5 recast code [77].

	Point (600, 10)L			Point (600, 10)R		
	SUSY	XQ-SDM	XQ-VDM	SUSY	XQ-SDM	XQ-VDM
efficiency	0.08898	0.07454	0.07752	0.08847	0.07531	0.07857
excl. XS [pb]	0.0535	0.0639	0.0612	0.0538	0.0631	0.0605
mass limit/SUSY XS	537	523	527	537	524	528
mass limit/XQ XS	705	688	692	704	689	693
1 – CLs	0.65	1	1	0.66	1	1

	Point (600, 300)L			Point (600, 300)R		
	SUSY	XQ-SDM	XQ-VDM	SUSY	XQ-SDM	XQ-VDM
efficiency	0.05183	0.04242	0.04159	0.05231	0.04281	0.04020
excl. XS [pb]	0.257	0.313	0.320	0.254	0.311	0.330
mass limit/SUSY XS	424	410	409	424	411	407
mass limit/XQ XS	563	547	545	564	547	542
1 – CLs	0.13	0.67	0.66	0.13	0.68	0.65

Table 12. Efficiencies, cross-sections excluded at 95% CL and corresponding extrapolated top-partner mass limits in GeV for the ATLAS gluino and squark search in the 2–6 jets channel, derived with the MADANALYSIS 5 recast code [77]. The last entry is the CLs exclusion value. The most sensitive SR is 4jl for the (600, 10) mass combination and 4jlm for the (600, 300) mass combination. Note that for this search the efficiencies strongly depend on the top-partner mass, so the extrapolation of the mass limit is unreliable; this is to large extent due to the cut on M_{eff} .

Table 12 summarises the total efficiencies in the most important SRs of this analysis together with the cross-sections excluded at 95% CL and the corresponding estimated top-partner mass limits for all four benchmark scenarios. We observe about 20% difference in the excluded cross-sections between SUSY and XQ interpretations. However, the mass limits derived from the excluded cross-sections are not reliable because for this search the total efficiencies strongly depend on the top-partner mass. As we will see in the next section, while this analysis does provide a limit on $T\bar{T}$ production because of the larger cross-section, it is not sensitive to $\tilde{t}_1\tilde{t}_1^*$ production.

5 Results in the top-partner versus DM mass plane

Having analysed the differences, or lack thereof, in the cut efficiencies of the experimental analyses for our four benchmark points, we next perform a scan in the plane of top-partner versus DM mass to derive the 95% CL exclusion lines. For definiteness, we keep the couplings fixed to the same values as for the (600, 10)L and (600, 10)R benchmark points.

Figure 5 presents the results for the ATLAS fully hadronic stop search implemented in CHECKMATE (top row), the CMS 1-lepton stop search recast with MAD-ANALYSIS 5 (middle row) and the ATLAS stop search in the 2-lepton final state recast with CHECKMATE (bottom row). The left panels are for the couplings of Point (600, 10)L, the right panels for the couplings of Point (600, 10)R, see Table 1. Shown are the 95% CL exclusion lines obtained from SUSY, XQ-SDM and XQ-VDM event simulation (dashed black, full black and full grey lines, respectively), as well as the exclusion lines obtained from rescaling SUSY efficiencies with XQ cross-sections (dotted black line). For each bin, the most sensitive SR used for the limit setting in the SUSY, XQ-SDM and XQ-VDM case is indicated by a coloured symbol as shown in the plot legends. For reference, the official ATLAS/CMS exclusion lines are also shown as full red lines.

For the CMS 1-lepton search, our exclusion line for left stops agrees remarkably well with the official CMS line (from the cut-based analysis). This is somewhat accidental, as *i)* the official CMS limit is for unpolarised stops, and *ii)* in our simulation the limit is mostly obtained from a SR optimised for decays to bottom and chargino, not from one optimised for decays to top and neutralino. On the other hand, the fairly large discrepancy for the ATLAS 2-lepton search is explained by the fact that the official exclusion curve was obtained using an MVA not available in CHECKMATE.

We see that over most of the mass plane, the best SR is the same for SUSY, XQ-SDM and XQ-VDM. (For the points where they are different, the sensitivities of the best and 2nd best SRs are actually quite similar.) The main conclusions which can be inferred from the plots are the following:

1. There are no significant differences between the XQ scenarios where the top partner decays to scalar or vector DM. This is expected because in the narrow-width approximation the process is largely dominated by the resonant contribution, the cross-section of which can be factorised into production cross-section times branching ratios. Since in our framework the branching ratios are 100% in the $t + \text{DM}$ channel, there are no relevant differences between different DM hypotheses.
2. The contours obtained by rescaling the SUSY efficiencies with the XQ cross-sections coincide quite well with the “true” XQ exclusion lines obtained by

simulating XQ events. This means, efficiency maps or cross-section upper limit maps for the stop–neutralino simplified model can safely be applied to the XQ case under consideration in this paper. It would thus be of advantage if the official maps by ATLAS and CMS extended to high enough masses to cover the 95% CL reach for fermionic top partners, which is currently not the case.

The situation is different for the generic gluino/squark search in the multi-jet + E_T^{miss} channel shown in Fig. 6.¹¹ Contrary to the estimated stop mass limit of about 400–500 GeV in Table 12, in the scan we do not obtain any limit on stops from this analysis. As already mentioned in Section 4.4, the reason is that the efficiency of the M_{eff} cut strongly depends on the overall mass scale, rendering the extrapolation of the limit unreliable. This can also be seen from the fact that the most sensitive SR changes more rapidly with the top-partner mass, see the colour code in Fig. 6. (The CHECKMATE implementation of the same analysis gives slightly stronger constraints on the SUSY case, excluding the region $m_{\tilde{t}} \approx 300 - 400$ GeV and $m_{\tilde{\chi}_1^0} \lesssim 50$ GeV, see the Appendix.) Likewise, also the limit for the XQ case derived from the scan differs from the estimated one in Table 12, although here the effect goes in the opposite direction: the actual limit is stronger than the extrapolated one. In fact, due to the increased efficiencies at high mass scales, this search can give stronger constraints on the XQ case than the stop searches, extending the limit up to $m_T \approx 900\text{--}950$ GeV for $m_{\text{DM}} \lesssim 300$ GeV. The naive rescaling of SUSY efficiencies with XQ cross-sections (dashed lines) however somewhat overestimates the reach for the XQ scenario. For this kind of analysis it will thus be interesting to produce efficiency maps specifically for the XQ model.

¹¹To produce this figure, we have extended the MADANALYSIS 5 recast code with the SRs 2j1, 4jm and 6jm, which are not present in the PAD version [77]. We note, however, that these SRs could not be validated, as no cut-flows or kinematic distributions are available for them from ATLAS.

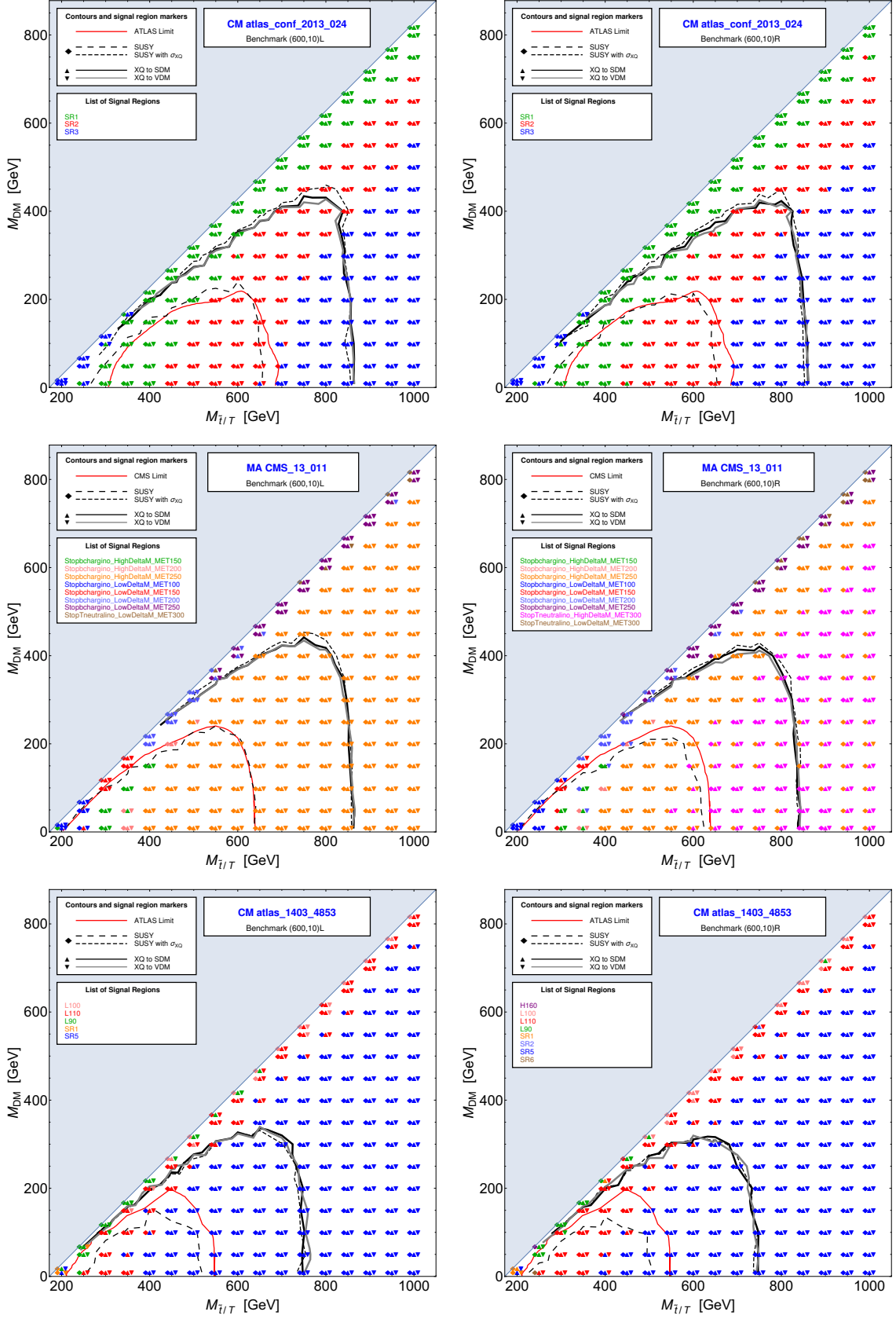


Figure 5. Comparisons of constraints in the top-partner versus DM mass plane for the fully hadronic stop search from ATLAS recast with CHECKMATE (top), the 1-lepton stop search from CMS recast with MADANALYSIS 5 (middle), and the 2-lepton stop search from ATLAS recast with CHECKMATE (bottom). See text for details.

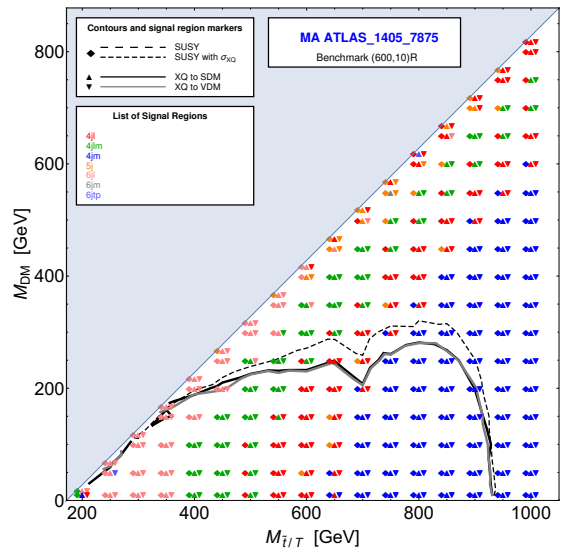


Figure 6. Comparison of constraints in the top-partner versus DM mass plane based on the MADANALYSIS5 recast code for the ATLAS gluino/squark search with 2–6 jets. As in Fig. 5, the various lines indicate the regions excluded at 8 TeV for the SUSY and XQ cases, and for the case where the SUSY efficiencies are applied to the XQ cross-sections. The plots also contain the information which SRs are the most sensitive ones for each point of the scan. Note that no stop–neutralino mass limit is obtained from this analysis.

6 Conclusions

We have studied how various analyses targeting $t\bar{t} + E_T^{\text{miss}}$ signatures, carried out by ATLAS and CMS in the context of SUSY searches, perform for models with fermionic top partners. Taking a simplified XQ model with one extra T quark and one DM state and comparing it to a simplified stop–neutralino model, we found that given the same kinematical configuration, SUSY and XQ efficiencies are very similar. The situation is different for generic multi-jet + E_T^{miss} searches targeting light-flavour squark and gluino production: here we found larger efficiencies for the SUSY than for the XQ case.

Putting everything together, we conclude that cross-section upper limit maps and efficiency maps obtained for stop simplified models in stop searches can also be applied to analogous models with fermionic top partners and a DM candidate, provided the narrow-width approximation applies. An exception may be the region of very small mass differences, where uncertainties in the total cut efficiencies become sizeable, though this does not influence much the actual limit.¹² To fully exploit the applicability to different top partner models, we encourage the experimental collaborations to present their cross-section upper limit and efficiency maps for a wide enough mass range, covering not only the reach for stops but also the reach for fermionic top partners. For the generic multi-jet + E_T^{miss} searches, on the other hand, it would be worthwhile to have efficiency maps specifically for the XQ model. As a service to the reader and potential user of our work, we provide the efficiency maps which we derived with CHECKMATE and MADANALYSIS 5 as auxiliary material [80]. The numbers of expected background and observed events from the experimental analyses, needed for the statistical interpretation, are summarized in Appendix B.

The similarity of SUSY and XQ efficiencies also means that, should a signal be observed in $t\bar{t} + E_T^{\text{miss}}$ events, it is not immediately obvious whether it comes from scalar or fermionic top partners. Since the production cross-section (assumed here to be pure QCD) is significantly larger for fermionic than for scalar top partners, one way of discrimination may be to correlate the effective mass scale, M_{eff} , or the effective transverse mass [81], with the observed number of events, see Fig. 7 for an illustrative example. (This was also observed in [82]. However, as pointed out in [18], for small XQ–DM mass splittings the decay products become softer and the discrimination from the SUSY case by cross-section and M_{eff} is lost.) Moreover, in the case of fermionic top partners, a corroborating signal may show up in generic gluino/squark searches, which have much less sensitivity to scalar top partners. Fi-

¹²However, this region could become important for scenarios in which multiple degenerate or nearly-degenerate top-partners occur, as in this case the cross-section might be enhanced by interference effects. Separate efficiency maps for the scalar or fermionic top partners would therefore be useful in this regime.

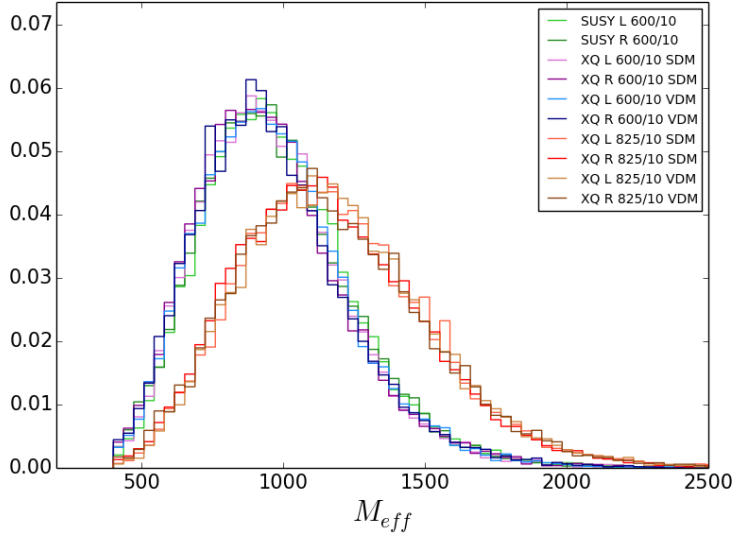


Figure 7. Comparison of the M_{eff} distributions for SUSY and XQ scenarios, after preselection cuts of the CMS 1-lepton stop search [21]. Here, M_{eff} is computed as $\sum p_T(\text{jets}) + p_T(l) + E_T^{\text{miss}}$. The green, violet and blue histograms are for the default (600, 10) benchmark points, while the orange and brown histograms show XQ scenarios that would give roughly the same visible cross-sections as the (600, 10) SUSY cases.

nally, the distinction between the two scenarios may be refined by considering special kinematic distributions as discussed in [83–85].

Acknowledgments

We thank Daniel Schmeier and Jamie Tattersall for help with CHECKMATE, and Benjamin Fuks and Dipan Sengupta for help with MADANALYSIS 5.

This research was supported in part by the “Investissements d’avenir, Labex ENIGMASS”, the ANR project DMASTROLHC grant no. ANR-12-BS05-0006 and the Theory-LHC-France initiative of the CNRS (INP/IN2P3). SK thanks the KITP Santa Barbara, supported by the National Science Foundation under Grant No. NSF PHY11-25915, for hospitality during part of the work.

A Additional CheckMATE results

As mentioned in Section 4, the ATLAS analyses [20] (1-lepton stop) and [23] (2–6 jets gluino/squark) are also implemented in CHECKMATE. For completeness, we show in Fig. 8 the CHECKMATE results for these two analyses together with the constraints obtained when considering all CHECKMATE ATLAS analyses simultaneously.

For the 1-lepton stop search from ATLAS, top row in Fig. 8, we note that the official SUSY limit is less well reproduced than for the corresponding CMS search recast with MADANALYSIS 5, cf. the middle row of plots in Fig. 5. This is expected, as the signal region `tn_boost` of the ATLAS search, which is optimised for high mass scales and boosted tops and is indeed the most sensitive SR for stop masses around 600 GeV, is not implemented in CHECKMATE. Moreover, there is a larger dependence on the top polarisation, as can be seen from the limit curves but also from the colour codes identifying the most sensitive SRs. Nonetheless, the resulting limit on XQs is very similar to that obtained from recasting the CMS search with MADANALYSIS 5. The fact that a stronger limit is obtained for \tilde{t}_R than for \tilde{t}_L was also mentioned in the experimental paper, see Fig. 24 in [20].

For the gluino/squark search in the 2–6 jets channel, middle row in Fig. 8, we observe some differences with respect to the corresponding MADANALYSIS 5 results in Fig. 6 in what concerns the best SRs. This can occur when several SRs have comparable sensitivity. The final 95% CL limit curves for XQs are however very similar in CHECKMATE and MADANALYSIS 5. The main difference is that the CHECKMATE implementation gives a small exclusion for the SUSY case in the range $m_{\tilde{t}_1} \approx 300\text{--}400$ GeV and $m_{\tilde{\chi}_1^0} \lesssim 50$ GeV, while with MADANALYSIS 5 one obtains only about 80–90% CL exclusion in this region.

Running all CHECKMATE ATLAS analyses simultaneously, one finds that up to top partner masses of about 700 GeV, the 1-lepton stop search [20] is always more sensitive than the hadronic stop search from the conference note [19]. (Although from the top row of plots in Fig. 5 the hadronic analysis seems to give the stronger limit, this comes from the fact that less events were observed in the three SRs of [19] than expected; comparing the expected limits, the search in the 1-lepton channel gives the stronger constraint.) It is thus [20] which is used for the limit setting in this mass range. Above $m_T \approx 700$ GeV, the gluino/squark in the 2–6 jets channel [23] is the most sensitive analysis and used for the limit setting.

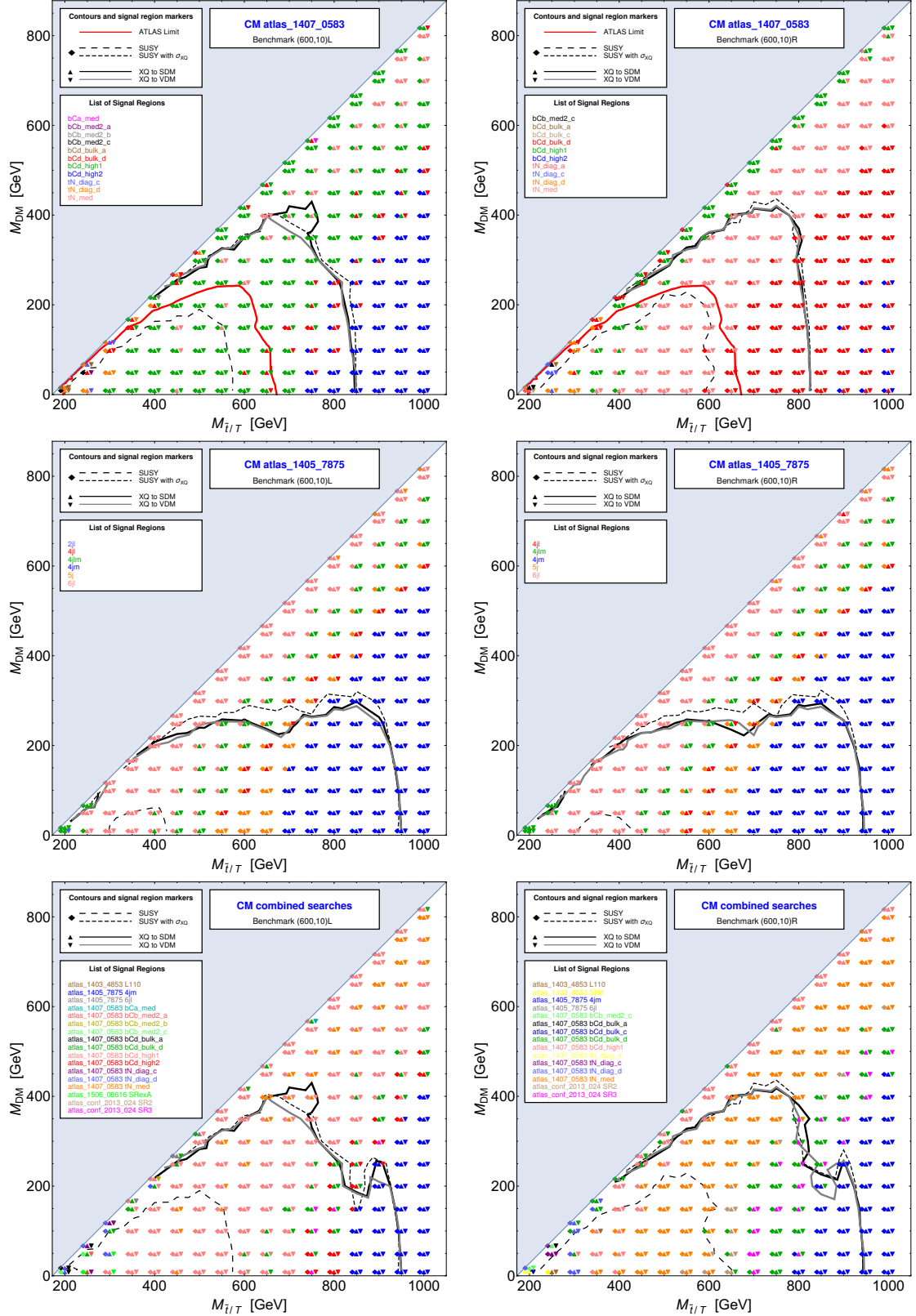


Figure 8. Additional comparison of constraints in the top-partner versus DM mass plane based on ATLAS analyses implemented in CHECKMATE: 1-lepton stop search [20] (top row), generic gluino/squark search [77] (middle row) and combination of all CHECKMATE ATLAS analyses (bottom row). As before, the left panels are for the couplings of Point (600,10)L, the right panels for the couplings of Point (600,10)R.

B Experimental data

For convenience, we here list in Tables 13–17 the numbers of expected background and numbers of observed events from the experimental analyses used in this paper.

Signal Region	# expected events	# observed events
SR1	17.5 ± 3.2	15
SR2	4.7 ± 1.5	2
SR3	2.7 ± 1.2	1

Table 13. Results from the fully hadronic stop search from ATLAS [19].

Signal Region	# expected events	# observed events
$\tilde{t}_1 \rightarrow t + \tilde{\chi}_1^0$, Low ΔM , $E_T^{\text{miss}} > 150$ GeV	251 ± 50	227
$\tilde{t}_1 \rightarrow t + \tilde{\chi}_1^0$, Low ΔM , $E_T^{\text{miss}} > 200$ GeV	83 ± 21	69
$\tilde{t}_1 \rightarrow t + \tilde{\chi}_1^0$, Low ΔM , $E_T^{\text{miss}} > 250$ GeV	31 ± 8	21
$\tilde{t}_1 \rightarrow t + \tilde{\chi}_1^0$, Low ΔM , $E_T^{\text{miss}} > 300$ GeV	11.5 ± 3.6	9
$\tilde{t}_1 \rightarrow t + \tilde{\chi}_1^0$, High ΔM , $E_T^{\text{miss}} > 150$ GeV	29 ± 7	23
$\tilde{t}_1 \rightarrow t + \tilde{\chi}_1^0$, High ΔM , $E_T^{\text{miss}} > 200$ GeV	17 ± 5	11
$\tilde{t}_1 \rightarrow t + \tilde{\chi}_1^0$, High ΔM , $E_T^{\text{miss}} > 250$ GeV	9.5 ± 2.8	3
$\tilde{t}_1 \rightarrow t + \tilde{\chi}_1^0$, High ΔM , $E_T^{\text{miss}} > 300$ GeV	4.7 ± 1.4	2
$\tilde{t}_1 \rightarrow b + \tilde{\chi}_1^+$, Low ΔM , $E_T^{\text{miss}} > 100$ GeV	1662 ± 203	1624
$\tilde{t}_1 \rightarrow b + \tilde{\chi}_1^+$, Low ΔM , $E_T^{\text{miss}} > 150$ GeV	537 ± 75	487
$\tilde{t}_1 \rightarrow b + \tilde{\chi}_1^+$, Low ΔM , $E_T^{\text{miss}} > 200$ GeV	180 ± 28	151
$\tilde{t}_1 \rightarrow b + \tilde{\chi}_1^+$, Low ΔM , $E_T^{\text{miss}} > 250$ GeV	66 ± 13	52
$\tilde{t}_1 \rightarrow b + \tilde{\chi}_1^+$, High ΔM , $E_T^{\text{miss}} > 100$ GeV	79 ± 12	90
$\tilde{t}_1 \rightarrow b + \tilde{\chi}_1^+$, High ΔM , $E_T^{\text{miss}} > 150$ GeV	38 ± 7	39
$\tilde{t}_1 \rightarrow b + \tilde{\chi}_1^+$, High ΔM , $E_T^{\text{miss}} > 200$ GeV	19 ± 5	18
$\tilde{t}_1 \rightarrow b + \tilde{\chi}_1^+$, High ΔM , $E_T^{\text{miss}} > 250$ GeV	9.9 ± 2.7	5

Table 14. Results from the 1-lepton stop search from CMS [21].

Signal Region	# expected events	# observed events
tN_med	13 ± 2.2	12
tN_high	5 ± 1	5
bCa_low	6.5 ± 1.4	11
bCa_med	17 ± 4	20
bCb_med1	32 ± 5	41
bCb_high	9.8 ± 1.6	7
bCc_diag	470 ± 50	493
bCd_high1	11.0 ± 1.5	16
bCd_high2	4.4 ± 0.8	5
tNbC_mix	7.2 ± 1	10
tN_diag_a	136 ± 22	117
tN_diag_b	152 ± 20	163
tN_diag_c	98 ± 13	101
tN_diag_d	236 ± 29	217
bCb_med2_a	12.1 ± 2.0	10
bCb_med2_b	7.4 ± 1.4	10
bCb_med2_c	21 ± 4	16
bCb_med2_d	9.1 ± 1.6	9
bCd_bulk_a	133 ± 22	144
bCd_bulk_b	73 ± 8	78
bCd_bulk_c	66 ± 6	61
bCd_bulk_d	26.5 ± 2.6	29
threeBody_a	16.9 ± 2.8	12
threeBody_b	8.4 ± 2.2	8
threeBody_c	35 ± 4	29
threeBody_d	29 ± 5	22

Table 15. Results from the 1-lepton stop search from ATLAS [20].

Signal Region	# expected events	# observed events
L90	300 ± 50	274
L100	5.2 ± 2.2	3
L110	9.3 ± 3.5	8
L120	19 ± 9	18
H160	26 ± 6	33
SR1	270 ± 40	250
SR2	3.4 ± 1.8	1
SR3	1.3 ± 0.6	2
SR4	3.7 ± 2.7	3
SR5	0.5 ± 0.4	0
SR6	3.8 ± 1.6	3
SR7	15 ± 7	15

Table 16. Results from 2-lepton stop search from ATLAS [22].

Signal Region	# expected events	# observed events
2jl	13000 ± 1000	12315
2jm	760 ± 50	715
2jt	125 ± 10	133
3j	5.0 ± 1.2	7
4jlm	2120 ± 110	2169
4jl	630 ± 50	608
4jm	37 ± 6	24
4jt	2.5 ± 1.0	0
5j	126 ± 13	121
6jl	111 ± 11	121
6jm	33 ± 6	39
6jt	5.2 ± 1.4	5
6jtp	4.9 ± 1.6	6

Table 17. Results from the generic squark and gluino search from ATLAS [23].

References

- [1] **ATLAS** Collaboration, G. Aad et al., *Observation of a new particle in the search for the Standard Model Higgs boson with the ATLAS detector at the LHC*, *Phys. Lett. B* **716** (2012) 1–29, [[arXiv:1207.7214](#)].
- [2] **CMS** Collaboration, S. Chatrchyan et al., *Observation of a new boson at a mass of 125 GeV with the CMS experiment at the LHC*, *Phys. Lett. B* **716** (2012) 30–61, [[arXiv:1207.7235](#)].
- [3] S. P. Martin, *A Supersymmetry primer*, [hep-ph/9709356](#). [Adv. Ser. Direct. High Energy Phys.18,1(1998)].
- [4] M. Drees, R. Godbole, and P. Roy, *Theory and phenomenology of sparticles: An account of four-dimensional $N=1$ supersymmetry in high energy physics*, World Scientific, 2004.
- [5] H. Baer and X. Tata, *Weak scale supersymmetry: From superfields to scattering events*, Cambridge University Press, 2006.
- [6] <https://twiki.cern.ch/twiki/bin/view/AtlasPublic/SupersymmetryPublicResults>.
- [7] <https://twiki.cern.ch/twiki/bin/view/CMSPublic/PhysicsResultsSUS>.
- [8] I. Antoniadis, *A Possible new dimension at a few TeV*, *Phys.Lett. B* **246** (1990) 377–384.
- [9] T. Appelquist, H.-C. Cheng, and B. A. Dobrescu, *Bounds on universal extra dimensions*, *Phys.Rev. D* **64** (2001) 035002, [[hep-ph/0012100](#)].
- [10] G. Servant and T. M. P. Tait, *Is the lightest Kaluza-Klein particle a viable dark matter candidate?*, *Nucl. Phys. B* **650** (2003) 391–419, [[hep-ph/0206071](#)].
- [11] C. Csaki, C. Grojean, J. Hubisz, Y. Shirman, and J. Terning, *Fermions on an interval: Quark and lepton masses without a Higgs*, *Phys.Rev. D* **70** (2004) 015012, [[hep-ph/0310355](#)].
- [12] G. Cacciapaglia, A. Deandrea, and J. Llodra-Perez, *A Dark Matter candidate from Lorentz Invariance in 6D*, *JHEP* **1003** (2010) 083, [[arXiv:0907.4993](#)].
- [13] H.-C. Cheng and I. Low, *TeV symmetry and the little hierarchy problem*, *JHEP* **09** (2003) 051, [[hep-ph/0308199](#)].
- [14] H.-C. Cheng and I. Low, *Little hierarchy, little Higgses, and a little symmetry*, *JHEP* **08** (2004) 061, [[hep-ph/0405243](#)].
- [15] I. Low, *T parity and the littlest Higgs*, *JHEP* **10** (2004) 067, [[hep-ph/0409025](#)].
- [16] J. Hubisz and P. Meade, *Phenomenology of the littlest Higgs with T-parity*, *Phys. Rev. D* **71** (2005) 035016, [[hep-ph/0411264](#)].
- [17] J. Hubisz, P. Meade, A. Noble, and M. Perelstein, *Electroweak precision constraints on the littlest Higgs model with T parity*, *JHEP* **01** (2006) 135, [[hep-ph/0506042](#)].

- [18] H.-C. Cheng, I. Low, and L.-T. Wang, *Top partners in little Higgs theories with T-parity*, *Phys. Rev.* **D74** (2006) 055001, [[hep-ph/0510225](#)].
- [19] **ATLAS** Collaboration, *Search for direct production of the top squark in the all-hadronic $t\bar{t}$ + $e\text{miss}$ final state in 21 fb⁻¹ of p-p collisions at $\sqrt{s}=8$ TeV with the ATLAS detector*, [ATLAS-CONF-2013-024](#).
- [20] **ATLAS** Collaboration, G. Aad et al., *Search for top squark pair production in final states with one isolated lepton, jets, and missing transverse momentum in $\sqrt{s}=8$ TeV pp collisions with the ATLAS detector*, *JHEP* **11** (2014) 118, [[arXiv:1407.0583](#)].
- [21] **CMS** Collaboration, S. Chatrchyan et al., *Search for top-squark pair production in the single-lepton final state in pp collisions at $\sqrt{s} = 8$ TeV*, *Eur. Phys. J.* **C73** (2013), no. 12 2677, [[arXiv:1308.1586](#)].
- [22] **ATLAS** Collaboration, G. Aad et al., *Search for direct top-squark pair production in final states with two leptons in pp collisions at $\sqrt{s} = 8$ TeV with the ATLAS detector*, *JHEP* **06** (2014) 124, [[arXiv:1403.4853](#)].
- [23] **ATLAS** Collaboration, G. Aad et al., *Search for squarks and gluinos with the ATLAS detector in final states with jets and missing transverse momentum using $\sqrt{s} = 8$ TeV proton-proton collision data*, *JHEP* **09** (2014) 176, [[arXiv:1405.7875](#)].
- [24] M. Drees, H. Dreiner, D. Schmeier, J. Tattersall, and J. S. Kim, *CheckMATE: Confronting your Favourite New Physics Model with LHC Data*, *Comput. Phys. Commun.* **187** (2014) 227–265, [[arXiv:1312.2591](#)].
- [25] E. Conte, B. Dumont, B. Fuks, and C. Wymant, *Designing and recasting LHC analyses with MadAnalysis 5*, *Eur. Phys. J.* **C74** (2014), no. 10 3103, [[arXiv:1405.3982](#)].
- [26] B. Dumont, B. Fuks, S. Kraml, S. Bein, G. Chalons, E. Conte, S. Kulkarni, D. Sengupta, and C. Wymant, *Toward a public analysis database for LHC new physics searches using MADANALYSIS 5*, *Eur. Phys. J.* **C75** (2015), no. 2 56, [[arXiv:1407.3278](#)].
- [27] S. Kraml, S. Kulkarni, U. Laa, A. Lessa, W. Magerl, D. Proschofsky-Spindler, and W. Waltenberger, *SModelS: a tool for interpreting simplified-model results from the LHC and its application to supersymmetry*, *Eur. Phys. J.* **C74** (2014) 2868, [[arXiv:1312.4175](#)].
- [28] S. Kraml, S. Kulkarni, U. Laa, A. Lessa, V. Magerl, W. Magerl, D. Proschofsky-Spindler, M. Traub, and W. Waltenberger, *SModelS v1.0: a short user guide*, [arXiv:1412.1745](#).
- [29] D. Barducci, A. Belyaev, M. Buchkremer, G. Cacciapaglia, A. Deandrea, S. De Curtis, J. Marrouche, S. Moretti, and L. Panizzi, *Framework for Model Independent Analyses of Multiple Extra Quark Scenarios*, *JHEP* **12** (2014) 080, [[arXiv:1405.0737](#)].

- [30] D. Barducci, A. Belyaev, M. Buchkremer, J. Marrouche, S. Moretti, and L. Panizzi, *XQCAT: eXtra Quark Combined Analysis Tool*, *Comput. Phys. Commun.* **197** (2015) 263–275, [[arXiv:1409.3116](#)].
- [31] **CDF** Collaboration, T. Aaltonen et al., *Search for Production of Heavy Particles Decaying to Top Quarks and Invisible Particles in $p\bar{p}$ collisions at $\sqrt{s} = 1.96$ TeV*, *Phys. Rev. Lett.* **106** (2011) 191801, [[arXiv:1103.2482](#)].
- [32] **CDF** Collaboration, T. Aaltonen et al., *Search for New T' Particles in Final States with Large Jet Multiplicities and Missing Transverse Energy in $p\bar{p}$ Collisions at $\sqrt{s} = 1.96$ TeV*, *Phys. Rev. Lett.* **107** (2011) 191803, [[arXiv:1107.3574](#)].
- [33] **ATLAS** Collaboration, *Search for Anomalous Missing ET in $t\bar{t}$ Events*, [ATLAS-CONF-2011-036](#).
- [34] **CMS** Collaboration, *A search for the decays of a new heavy particle in multijet events with the razor variables at CMS in pp collisions at $\sqrt{s}=7$ TeV*, [CMS-PAS-SUS-12-009](#).
- [35] G. Cacciapaglia, A. Deandrea, J. Ellis, J. Marrouche, and L. Panizzi, *LHC Missing-Transverse-Energy Constraints on Models with Universal Extra Dimensions*, *Phys. Rev.* **D87** (2013), no. 7 075006, [[arXiv:1302.4750](#)].
- [36] L. Edelhäuser, M. Krämer, and J. Sonneveld, *Simplified models for same-spin new physics scenarios*, *JHEP* **04** (2015) 146, [[arXiv:1501.03942](#)].
- [37] C. Arina, M. E. C. Catalan, S. Kraml, S. Kulkarni, and U. Laa, *Constraints on sneutrino dark matter from LHC Run 1*, *JHEP* **05** (2015) 142, [[arXiv:1503.02960](#)].
- [38] S. Baek, P. Ko and P. Wu, *Top-philic Scalar Dark Matter with a Vector-like Fermionic Top Partner*, [arXiv:1606.00072](#).
- [39] T. Gajdosik, R. M. Godbole, and S. Kraml, *Fermion polarization in sfermion decays as a probe of CP phases in the MSSM*, *JHEP* **09** (2004) 051, [[hep-ph/0405167](#)].
- [40] P. Z. Skands et al., *SUSY Les Houches accord: Interfacing SUSY spectrum calculators, decay packages, and event generators*, *JHEP* **07** (2004) 036, [[hep-ph/0311123](#)].
- [41] Q. H. Cao, C. S. Li and C.-P. Yuan, *Impact of Single-Top Measurement to Littlest Higgs Model with T-Parity*, *Phys. Lett. B* **668** (2008) 24 [[hep-ph/0612243](#)].
- [42] M. M. Nojiri and M. Takeuchi, *Study of the top reconstruction in top-partner events at the LHC*, *JHEP* **0810** (2008) 025 [[arXiv:0802.4142](#) [[hep-ph](#)]].
- [43] J. Shelton, *Polarized tops from new physics: signals and observables*, *Phys. Rev.* **D79** (2009) 014032 [[arXiv:0811.0569](#)].
- [44] M. Perelstein and A. Weiler, *Polarized Tops from Stop Decays at the LHC*, *JHEP* **0903** (2009) 141 [[arXiv:0811.1024](#)].
- [45] E. L. Berger, Q. H. Cao, J. H. Yu and H. Zhang, *Measuring Top Quark Polarization*

- in *Top Pair plus Missing Energy Events*, *Phys. Rev. Lett.* **109** (2012) 152004 [[arXiv:1207.1101](#)].
- [46] C.-Y. Chen, A. Freitas, T. Han, and K. S. M. Lee, *New Physics from the Top at the LHC*, *JHEP* **11** (2012) 124, [[arXiv:1207.4794](#)].
 - [47] B. Bhattacharjee, S. K. Mandal and M. Nojiri, *Top Polarization and Stop Mixing from Boosted Jet Substructure*, *JHEP* **1303** (2013) 105 [[arXiv:1211.7261](#)].
 - [48] G. Belanger, R. M. Godbole, L. Hartgring, and I. Niessen, *Top Polarization in Stop Production at the LHC*, *JHEP* **05** (2013) 167, [[arXiv:1212.3526](#)].
 - [49] I. Low, *Polarized charginos (and top quarks) in scalar top quark decays*, *Phys. Rev.* **D88** (2013) no.9, 095018 [[arXiv:1304.0491](#)].
 - [50] G. Belanger, R. M. Godbole, S. Kraml, and S. Kulkarni, *Top Polarization in Sbottom Decays at the LHC*, [arXiv:1304.2987](#).
 - [51] K. Wang, L. Wang, T. Xu and L. Zhang, *Polarization effects in early SUSY searches at the CERN LHC*, *Eur. Phys. J.* **C75** (2015) no.6, 285 [[arXiv:1312.1527](#)].
 - [52] **ATLAS** Collaboration, G. Aad et al., *ATLAS Run 1 searches for direct pair production of third-generation squarks at the Large Hadron Collider*, *Eur. Phys. J.* **C75** (2015), no. 10 510, [[arXiv:1506.08616](#)].
 - [53] **CMS** Collaboration, *Search for top squarks decaying to a charm quark and a neutralino in events with a jet and missing transverse momentum*, [CMS-PAS-SUS-13-009](#).
 - [54] **CMS** Collaboration, S. Chatrchyan et al., *Search for new physics in the multijet and missing transverse momentum final state in proton-proton collisions at $\sqrt{s}=8$ TeV*, *JHEP* **1406** (2014) 055, [[arXiv:1402.4770](#)].
 - [55] **CMS** Collaboration, *Exclusion limits on gluino and top-squark pair production in natural SUSY scenarios with inclusive razor and exclusive single-lepton searches at 8 TeV*, [CMS-PAS-SUS-14-011](#).
 - [56] **CMS** Collaboration, *Search for direct production of top squark pairs decaying to all-hadronic final states in pp collisions at $\sqrt{s}=13$ TeV*, [CMS-PAS-SUS-16-007](#).
 - [57] A. Djouadi, J.-L. Kneur, and G. Moultaka, *SuSpect: A Fortran code for the supersymmetric and Higgs particle spectrum in the MSSM*, *Comput. Phys. Commun.* **176** (2007) 426–455, [[hep-ph/0211331](#)].
 - [58] J. Alwall, M. Herquet, F. Maltoni, O. Mattelaer, and T. Stelzer, *MadGraph 5 : Going Beyond*, *JHEP* **1106** (2011) 128, [[arXiv:1106.0522](#)].
 - [59] J. Alwall, R. Frederix, S. Frixione, V. Hirschi, F. Maltoni, O. Mattelaer, H. S. Shao, T. Stelzer, P. Torrielli, and M. Zaro, *The automated computation of tree-level and next-to-leading order differential cross sections, and their matching to parton shower simulations*, *JHEP* **07** (2014) 079, [[arXiv:1405.0301](#)].

- [60] T. Sjostrand, S. Mrenna, and P. Z. Skands, *PYTHIA 6.4 Physics and Manual*, *JHEP* **0605** (2006) 026, [[hep-ph/0603175](#)].
- [61] R. Boughezal and M. Schulze, *$t\bar{t}$ +large missing energy from top-quark partners: A comprehensive study at next-to-leading order QCD*, *Phys. Rev.* **D88** (2013), no. 11 114002, [[arXiv:1309.2316](#)].
- [62] A. Alloul, N. D. Christensen, C. Degrande, C. Duhr, and B. Fuks, *FeynRules 2.0 - A complete toolbox for tree-level phenomenology*, *Comput. Phys. Commun.* **185** (2014) 2250–2300, [[arXiv:1310.1921](#)].
- [63] J. Pumplin, D. Stump, J. Huston, H. Lai, P. M. Nadolsky, et al., *New generation of parton distributions with uncertainties from global QCD analysis*, *JHEP* **0207** (2002) 012, [[hep-ph/0201195](#)].
- [64] J. de Favereau, C. Delaere, P. Demin, A. Giammanco, V. Lemaître, et al., *DELPHES 3, A modular framework for fast simulation of a generic collider experiment*, [arXiv:1307.6346](#).
- [65] http://pauli.uni-muenster.de/~akule_01/nllwiki/index.php/NLL-fast.
- [66] W. Beenakker, R. Hopker, M. Spira, and P. Zerwas, *Squark and gluino production at hadron colliders*, *Nucl.Phys.* **B492** (1997) 51–103, [[hep-ph/9610490](#)].
- [67] A. Kulesza and L. Motyka, *Threshold resummation for squark-antisquark and gluino-pair production at the LHC*, *Phys.Rev.Lett.* **102** (2009) 111802, [[arXiv:0807.2405](#)].
- [68] A. Kulesza and L. Motyka, *Soft gluon resummation for the production of gluino-gluino and squark-antisquark pairs at the LHC*, *Phys.Rev.* **D80** (2009) 095004, [[arXiv:0905.4749](#)].
- [69] W. Beenakker, S. Brensing, M. Kramer, A. Kulesza, E. Laenen, et al., *Soft-gluon resummation for squark and gluino hadroproduction*, *JHEP* **0912** (2009) 041, [[arXiv:0909.4418](#)].
- [70] W. Beenakker, S. Brensing, M. Kramer, A. Kulesza, E. Laenen, et al., *Squark and Gluino Hadroproduction*, *Int.J.Mod.Phys.* **A26** (2011) 2637–2664, [[arXiv:1105.1110](#)].
- [71] W. Beenakker, M. Kramer, T. Plehn, M. Spira, and P. Zerwas, *Stop production at hadron colliders*, *Nucl.Phys.* **B515** (1998) 3–14, [[hep-ph/9710451](#)].
- [72] W. Beenakker, S. Brensing, M. Kramer, A. Kulesza, E. Laenen, et al., *Supersymmetric top and bottom squark production at hadron colliders*, *JHEP* **1008** (2010) 098, [[arXiv:1006.4771](#)].
- [73] M. Cacciari, M. Czakon, M. Mangano, A. Mitov, and P. Nason, *Top-pair production at hadron colliders with next-to-next-to-leading logarithmic soft-gluon resummation*, *Phys.Lett.* **B710** (2012) 612–622, [[arXiv:1111.5869](#)].
- [74] M. Cacciari and G. P. Salam, *Dispelling the N^3 myth for the k_t jet-finder*, *Phys. Lett.* **B641** (2006) 57–61, [[hep-ph/0512210](#)].

- [75] M. Cacciari, G. P. Salam, and G. Soyez, *FastJet User Manual*, *Eur. Phys. J.* **C72** (2012) 1896, [[arXiv:1111.6097](#)].
- [76] B. Dumont, B. Fuks, and C. Wymant, *MadAnalysis 5 implementation of CMS-SUS-13-011: search for stops in the single lepton final state at 8 TeV*, doi:[10.7484/INSPIREHEP.DATA.LR5T.2RR3](#), (validation material in [http://madanalysis.irmp.ucl.ac.be/raw-attachment/wiki/PublicAnalysisDatabase/ma5_validation_CMS-SUS-13-011.pdf](#))
- [77] G. Chalons and D. Sengupta, *MadAnalysis 5 implementation of the ATLAS multi jet analysis documented in arXiv:1405.7875*, *JHEP* **1409** (2014) 176, doi:[10.7484/INSPIREHEP.DATA.UYT6.GFD9](#).
- [78] **ATLAS** Collaboration, G. Aad et al., *Search for direct pair production of the top squark in all-hadronic final states in proton-proton collisions at $\sqrt{s} = 8$ TeV with the ATLAS detector*, *JHEP* **09** (2014) 015, [[arXiv:1406.1122](#)].
- [79] J. Cao, L. Shang, J. M. Yang, and Y. Zhang, *Explanation of the ATLAS Z-Peaked Excess in the NMSSM*, *JHEP* **06** (2015) 152, [[arXiv:1504.07869](#)].
- [80] The efficiency maps can be downloaded from [http://lpsc.in2p3.fr/projects-th/recasting/susy-vs-vlq/ttbarMET/](#)
- [81] M. E. Cabrera and J. A. Casas, *Understanding and improving the Effective Mass for LHC searches*, [arXiv:1207.0435](#).
- [82] A. Datta, G. L. Kane and M. Toharia, *Is it SUSY?*, [hep-ph/0510204](#).
- [83] T. Han, R. Mahbubani, D. G. E. Walker and L. T. Wang, *Top Quark Pair plus Large Missing Energy at the LHC*, *JHEP* **0905** (2009) 117 [[arXiv:0803.3820](#) [[hep-ph](#)]].
- [84] J. M. Smillie and B. R. Webber, *Distinguishing spins in supersymmetric and universal extra dimension models at the large hadron collider*, *JHEP* **10** (2005) 069, [[hep-ph/0507170](#)].
- [85] A. Datta, K. Kong, and K. T. Matchev, *Discrimination of supersymmetry and universal extra dimensions at hadron colliders*, *Phys. Rev.* **D72** (2005) 096006, [[hep-ph/0509246](#)]. [Erratum: *Phys. Rev.* **D72**, 119901(2005)].